Journal of Biomolecular Structure & Dynamics, ISSN 0739-1102
Volume 16, Issue Number 3, (1998)

The Solution Conformation of a Carbocyclic Analog of the Dickerson-Drew Dodecamer: Comparison with its own X-ray Structure and that of the NMR Structure of the Native Counterpart

http://www.albany.edu/chemistry/sarma/jbsd.html

Aleksej Yu. Denisov[1], E. V. Zamaratski[1], Tatiana V. Maltseva[1], Anders Sandström[1], Somer Bekiroglu[1], Karl-Heinz Altmann[2], Martin Egli[3] and Jyoti Chattopadhyaya[1]*

[1]Department of Bioorganic Chemistry, Box 581, Biomedical Center, University of Uppsala, S-751 23 Uppsala, Sweden
[2]Department of Oncology, Novartis Pharma Inc., CH-4002 Basel, Switzerland
[3]Drug Discovery Program, Department of Molecular Pharmacology and Biological Chemistry, Northwestern University Medical School, Chicago, IL 60611-3008, USA

Summary

The NMR conformation of a carbocyclic analog of the Dickerson-Drew dodecamer [d(CGCGAAT*T*CGCG)]$_2$ containing 6′-α-Me carbocyclic thymidines (T*) has been determined and compared with that of its X-ray structure. The solution structure of the 6′-α-Me carbocyclic thymidine modified duplex has also been compared with the solution structure of the corresponding unmodified Dickerson-Drew duplex solved by us under the same experimental conditions. The NMR structures have been based on 24 experimental distance and torsion constraints per residue for [d(CGCGAAT*T*CGCG)]$_2$ (**1**) and on 21 constraints per residue for the natural counterpart. In general, both final NMR structures are more close to the B-type DNA. The cyclopentane moieties of the carbocyclic thymidine residues adopt C1′-*exo* B-DNA type puckers (the phase angles P = 136-139° and the puckering amplitudes Ψ = 36-37°) that are close to their previously published crystal C1′-*exo* or C2′-*endo* puckers. The main differences between the two NMR structures are for β(T*8) and ε, ξ(T*7) backbone torsions (27-50°), for basepair twist for the 7-8 and 8-9 basepair steps (5-6°), tilt for the 8-9 step (7°), roll for the 7-8 step (7°), shift for the 7-8 step (0.9Å) and slide for the 9-10 step (0.6Å). The relatively small deviations of helical structure parameters lead to structural isomorphism of these duplexes in aqueous solutions (atomic RMSD = 1.0Å). The difference of the minor groove widths (less than 0.7Å) in the core part of the modified duplex in comparison with the native one is much smaller than the difference between the X-ray structures of these duplexes. A detailed comparison of NMR and X-ray structure parameters showed significant monotonic differences (0.9-2.5Å) for all basepair slides in both duplexes. Deviations between NMR and X-ray structure parameters for the modified duplex were also found for basepair tilt of the 4-5 step (13°), rolls for the 8-9 and 10-11 steps (16° and 19°), twist of the 3-4 step (8°) and shift of the 9-10 step (0.9Å).

Introduction

Owing to the insufficient stability and cellular penetration properties of natural oligo-DNA and -RNA, the chemically modified oligonucleotides (1,2) (and references therein) have played an important role in the design of the antisense and antigene therapy (3). Three important features in these chemically modified oligonucleotides are that they should bind strongly to the opposite strand, show resistance to the nucleolytic degradation and, ideally, should penetrate into the cell more easily than the natural counterpart. Although many modified oligonucleotides have so far been prepared and their binding data to the opposite DNA or RNA strand have been reported, very little information (4-6) is however available regarding how the structure of these covalently modified duplexes changes in aqueous solution vis-a-vis their natural counterpart, or what are the quantitative structural differences between the solution and the solid state structure of these modified duplexes.

Although the introduction of 6′-α-methyl-2′-deoxy-carbocyclic or 6′-α-hydroxy-

*Author to whom correspondence should be addressed. Phone: +46-18-4714577; Fax: +46-18-554495; E-mail: jyoti@bioorgchem.uu.se

2′-hydroxy-carbocyclic thymidine residues in the DNA duplex reduces the melting point of the duplex from 0.1° to 1.9° per modification depending on the sequence, we chose to study oligonucleotides containing carbocyclic analogs of 2′-deoxyribonucleotides because of the following reasons (1,2,7): (i) they exhibit greater

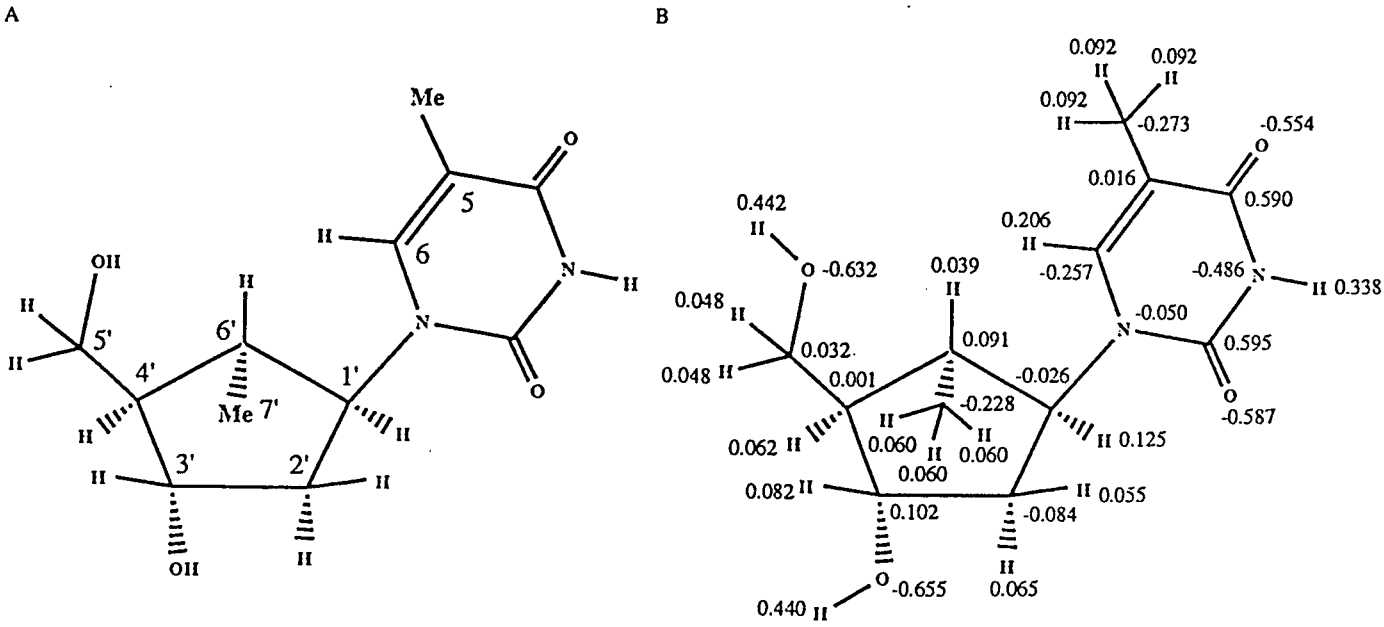

Figure 1: The structure of the 6′-α-Me carbocyclic thymidine with atomic numbers (panel **A**) and the atomic charges (panel **B**) resulting from the Gaussian 94 and RESP programs (see experimental part).

resistance to the enzymatic cleavage of the glycosidic linkage, (ii) they show improved resistance to cellular nucleases, and most importantly (iii) the X-ray crystal structure of two self-complementary DNA duplexes containing 6′-α-methyl- and 6′-α-hydroxy carbocyclic thymidines are available (2,7), which would enable us to compare their structures with those of the solution structures. The absence of stereoelectronic anomeric and gauche effects (8) renders the five-mem-

Table I

Proton and phosphorus chemical shifts (ppm) for duplexes (**1**) and (**2**) at 20°C[a].

Residue	Duplex	H6/H8	H5/Me/H2	H1′	H2′	H2″	H3′	H4′	H5′/H5″	^{31}P [b]
C1	(1)	7.71	5.98	5.83	2.05	2.49	4.78	4.14	3.80	-
	(2)	7.72	5.99	5.84	2.05	2.49	4.79	4.15	3.80	-
G2	(1)	8.03	-	5.98	2.74	2.81	5.06	4.43	4.18, 4.06	-4.08
	(2)	8.04	-	5.98	2.76	2.81	5.06	4.44	4.18, 4.07	-4.08
C3	(1)	7.38	5.45	5.67	2.02	2.41	4.91	4.24	4.26, 4.20	-4.16
	(2)	7.36	5.46	5.68	1.93	2.36	4.89	4.22	4.25, 4.20	-4.14
G4	(1)	7.95	-	5.63	2.77	2.89	5.10	4.42	4.19, 4.09	-3.96
	(2)	7.95	-	5.53	2.73	2.86	5.09	4.41	4.20, 4.08	-3.99
A5	(1)	8.10	7.49	6.15	2.69	3.03	5.14	4.51	4.29	-4.30
	(2)	8.20	7.31	6.09	2.79	3.03	5.16	4.55	4.28	-4.13
A6	(1)	8.20	7.75	5.95	2.71	2.53	5.11	4.48	4.31	-4.25
	(2)	8.21	7.71	6.25	2.65	3.02	5.11	4.56	4.35	-4.29
T*7	(1)	7.20	1.50	4.35	2.23	1.91	4.71	2.04	4.20, 4.03	-3.50
T7	(2)	7.20	1.35	6.00	2.07	2.66	4.91	4.30	4.44, 4.27	-4.43
T*8	(1)	7.42	1.58	4.64	2.12	2.32	4.72	2.01	4.16, 4.05	-3.03
T8	(2)	7.46	1.62	6.19	2.25	2.64	4.99	4.30	4.28, 4.20	-4.36
C9	(1)	7.56	5.68	5.83	2.09	2.50	4.89	4.23	4.20, 4.16	-3.82
	(2)	7.56	5.71	5.75	2.15	2.50	4.97	4.24	4.26, 4.20	-4.27
G10	(1)	7.99	-	5.93	2.70	2.78	5.05	4.44	4.19, 4.10	-4.14
	(2)	8.00	-	5.94	2.71	2.76	5.08	4.45	4.24, 4.13	-3.88
C11	(1)	7.40	5.50	5.82	1.98	2.40	4.89	4.23	4.27, 4.19	-4.10
	(2)	7.42	5.53	5.84	1.99	2.41	4.89	4.25	4.28, 4.21	-4.07
G12	(1)	8.02	-	6.23	2.70	2.45	4.75	4.25	4.15	-3.91
	(2)	8.03	-	6.24	2.69	2.45	4.77	4.26	4.16	-3.93

[a]Proton chemical shifts for H6′ and 6′-Me in duplex (**1**) are 1.48 and 1.00 (T*7), 1.99 and 1.16 ppm (T*8). The chemical shifts of imino protons for G2, G4, G10, T*7/T7, T*8/T8 are 13.17, 12.84, 13.00, 13.68, 13.58 ppm for duplex (**1**) and 13.15, 12.78, 12.98, 13.76, 13.89 for duplex (**2**) at 15°C.

[b]Phosphorus chemical shifts (for 5′-phosphate groups) are referenced to external trimethyl phosphate.

bered cyclopentane ring more flexible. Recent studies (2,7) of the X-ray structure of DNA duplexes showed that these carbocyclic residues can adjust smoothly to the geometrical constraints exerted by the furanosyl phosphate backbones and they are fully compatible with B-form DNA, with a slight enlarging of the minor groove in the former, which is relatively devoid of water molecules in the core, in part due to the bulky hydrophobic methyl groups (2).

We herein report the solution conformation of the modified dodecamer [d(CGCGAAT*T*CGCG)]$_2$ (**1**) with 6′-α-Me carbocyclic thymidines (T*, see Figure 1A) by NMR and molecular modeling and its comparison with the native Dickerson-Drew duplex [d(CGCGAATTCGCG)]$_2$ (**2**). We also show the structural differences between the solid state and the solution structures of the modified dodecamer [d(CGCGAAT*T*CGCG)]$_2$ (**1**), as was previously done for the natural Dickerson-Drew dodecamer duplex (4,9,10).

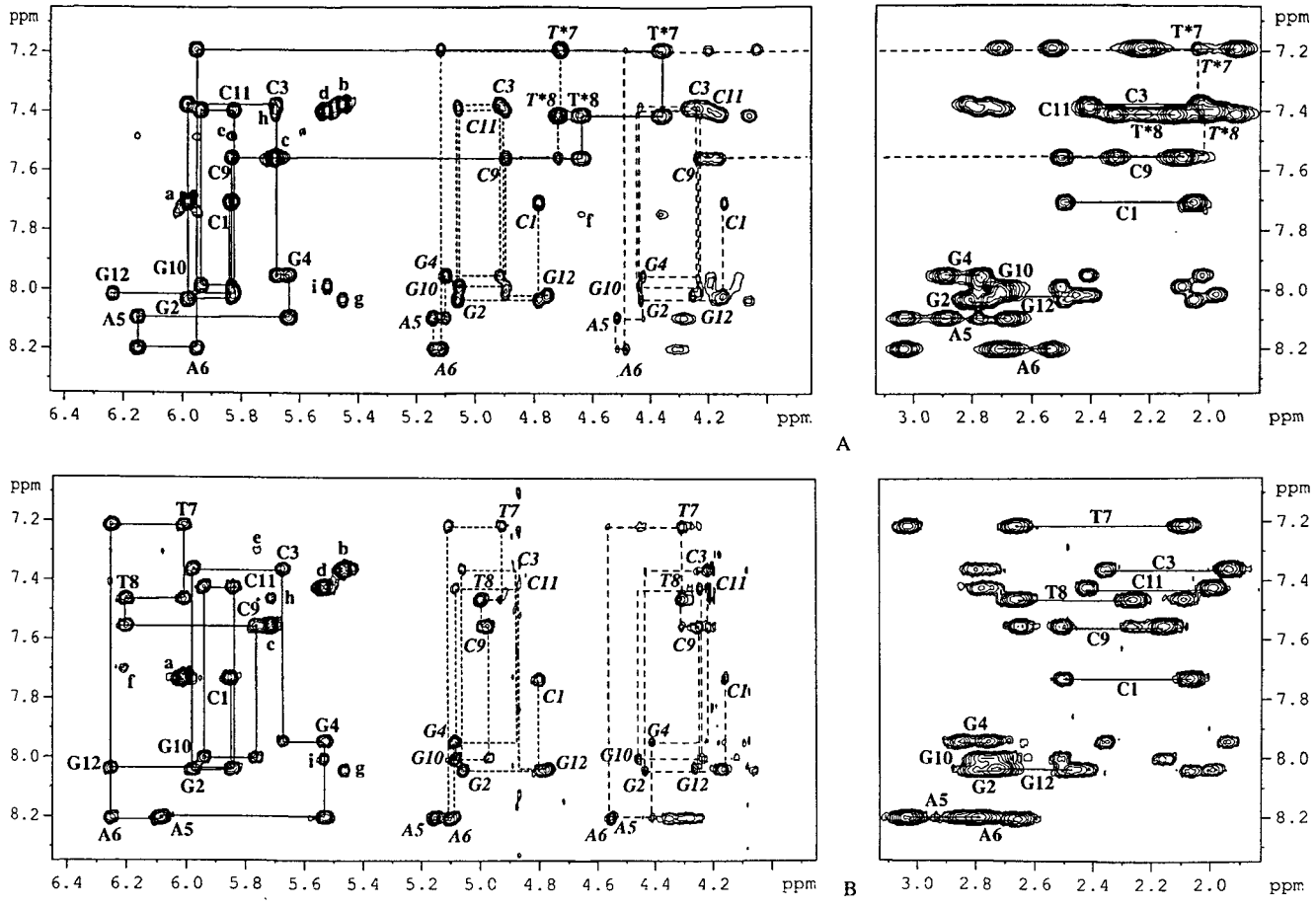

Figure 2: Expanded plots of NOESY spectra of duplex (**1**) (panel **A**, 600 MHz, 150 ms mixing time) and duplex (**2**) (panel **B**, 500 MHz, 200 ms) at 20°C. The assignments are shown in the NOESY spectra through H1′$_{(i)}$-H6/H8$_{(i)}$-H1′$_{(i-1)}$ pathway (solid lines) and also through similar pathways for H3′ and H4′ (dashed lines). The intraresidue H2′-H6/H8 and H2″-H6/H8 crosspeaks are connected by solid lines, and the intranucleotide crosspeaks are labeled by the residue name and number. The letters **a**, **b**, **c** and **d** in panels **A** and **B** correspond to the H5-H6 crosspeaks for C1, C3, C9 and C11, the letters **e** and **f** show the interstrand crosspeaks for H2(A5)-H1′ (C9) and H2(A6)-H1′ (T*8/T8), and the letters **g**, **h** and **i** mark interresidue intrastrand crosspeaks H8(G2)-H5(C3), H6(T8)-H5(C9) and H8(G10)-H5(C11), respectively.

Results and Discussion

(A) Resonance Assignment

The assignment of the non-exchangeable proton resonances in NOESY spectra of duplexes (**1**) and (**2**) was carried out in the usual sequential manner (11,12), which is normally used for right-handed DNA (Figure 2). The DQF-COSY and TOCSY spectra were also used to assign the sugar protons. The assignment of proton signals for natural duplex (**2**) is the same as in previously published works (4,9,10,13,14). The proton chemical shifts of both duplexes are presented in Table 1. The proton chemical shifts for duplexes (**1**) and (**2**) are significantly different for H1′, H2″ of A6 and H2″ of T*7. These H2″ proton signals have been shifted upfield by 0.5-0.7 ppm in the modified duplex (**1**), possibly due to the absence of the negatively charged O4′ sugar oxygen in the neighbouring residues. A few inter-

strand crosspeaks were found: H2(A5)-H1′(C9), H2(A6)-H1′(T8/T*8) and H2(A6)-6′Me(T*8) (Figures 3A and 3B).

The assignment of the imino protons was done from a NOESY spectrum by using the crosspeaks of NH(G) with NH_2(C) or NH(T) with H2(A) of complementary basepairs, as well as by crosspeaks between imino protons for neighbouring basepairs (11,12). The chemical shifts of the imino protons are presented in Table I (footnote). Only one of the imino protons is significantly shifted (*i.e.* T*8 by 0.3 ppm upfield) (Figure 3C) in duplex (**1**) in comparison with the native duplex (**2**), which simply could be due to the change of the chemical environment specially near carbocyclic moieties.

The sugar ring pucker and backbone β, γ and ε torsions were initially constrained by the observed $^3J_{HH}$, $^3J_{HP}$ and $^3J_{CP}$ in conjunction with the observed nOes (*vide infra*).

(B) Sugar Ring Pucker

The conformation of all sugar rings in both duplexes was determined from $^3J_{HH}$ coupling constants obtained from DQF-COSY experiments (Table II). The $^3J_{1'2'}$ and $^3J_{1'2''}$ in unmodified nucleotides were determined from H1′-H2″ crosspeak splittings (15) and the $^3J_{2'3'}$, $^3J_{2''3'}$ and $^3J_{3'4'}$ were extracted from sums of couplings (16), $\Sigma_{2'}$, $\Sigma_{2''}$ and $\Sigma_{3'}$. These coupling constants were refined by spectral simulations with the help of the NMRSIM program (v. 2.5, Bruker). A similar procedure of extracting coupling constants for both carbocyclic thymidines was initially applied to H1′-H2′/H2″/H6′ crosspeaks (Figure 4). It is noteworthy that the $^3J_{1'2'}$ and $^3J_{1'2''}$ for the carbocyclic moieties are much larger than for the corresponding natural counterpart since the electronegativity of the 6′-methine moiety is smaller than that of O4′. This electronegativity effect is accounted for by the PSEUROT program (17-19).

Table II

Coupling constants (Hz)a in duplexes (**1**) and (**2**) at 20°C and calculated best sugar puckers.

Residue	Duplex	$J_{1'2'}$	$J_{1'2''}$	$J_{2'3'}$	$J_{2''3'}$	$J_{3'4'}$	$J_{4'5'}+J_{4'5''}$	$J_{H3'P}$ [b]	P_S [c]	Ψ_S [c]	%S[c]
C1	(**1**)	9.4	5.3	5.9	2.5	3.3	8.4	5.2	135.2	41.9	81
	(**2**)	9.5	5.3	5.6	2.0	3.2	8.0	6.4	136.4	41.4	84
G2	(**1**)	9.9	5.6	4.8	0.5	1.5	-	2.5	163.8	35.8	97
	(**2**)	9.8	5.6	-	-	-	-	3.4	-	-	95
C3	(**1**)	9.5	5.6	5.5	1.5	2.5	3.8	4.2	145.8	36.8	88
	(**2**)	9.8	5.6	5.7	1.5	3.3	-	5.8	133.6	39.2	88
G4	(**1**)	9.8	5.9	4.8	0.5	1.5	3.4	2.1	169.4	35.3	97
	(**2**)	9.6	5.2	5.0	0.5	1.5	-	4.0	158.9	35.9	96
A5	(**1**)	9.8	5.9	5.1	1.0	1.7	3.0	1.8	161.4	35.1	94
	(**2**)	9.9	6.0	5.8	1.0	1.8	3.5	2.6	151.2	33.0	95
A6	(**1**)	9.9	5.8	5.3	1.0	1.8	2.9	2.9	155.2	35.0	94
	(**2**)	9.9	5.5	5.5	1.0	2.1	3.5	2.3	147.0	36.2	93
T*7	(**1**)	11.5	7.5	5.0	0.5	1.5	3.5	6.0	138.3	37.0	100
T7	(**2**)	9.7	6.0	6.0	1.5	3.0	3.9	2.3	136.4	35.3	90
T*8	(**1**)	11.0	8.5	5.0	0.5	1.5	3.0	3.5	136.9	33.2	100
T8	(**2**)	9.9	6.0	5.7	1.0	2.6	3.0	2.6	141.3	34.5	93
C9	(**1**)	9.4	5.3	5.5	1.0	2.3	3.6	3.5	146.1	36.3	91
	(**2**)	9.6	5.2	5.3	1.0	3.0	3.2	5.1	137.3	40.0	89
G10	(**1**)	9.9	5.6	4.8	0.5	1.5	-	2.5	163.8	35.8	97
	(**2**)	9.8	5.3	-	-	-	-	4.2	-	-	90
C11	(**1**)	9.5	5.6	5.5	1.0	2.3	-	3.5	147.4	35.2	91
	(**2**)	9.8	5.3	5.7	1.5	3.3	-	5.1	132.8	41.0	88
G12	(**1**)	9.5	5.2	5.1	2.9	2.6	2.9	d	149.6	43.4	80
	(**2**)	9.3	5.5	5.3	2.5	2.5	3.1	d	151.1	39.8	82

[a]±0.5Hz for $J_{1'2'}$ or $J_{1'2''}$ and ±1.0 Hz for other coupling constants. Values of $J_{1'6'}$, $J_{4'6'}$ and $J_{6'\text{-Me}}$ in duplex (**1**) are 10.5, 7.5 and 5.0 (T*7); 9.5, 8.0 and 5.0 Hz (T*8), respectively.

[b]The J_{HP} coupling constants were extracted from DQF-COSY spectra for duplex (**1**) and were taken from previous work (Sclenar & Bax, 1987) for duplex (**2**).

[c]From program PSEUROT (17-19) or by the equation(16) $\%S = (\Sigma_{1'} - 9.8)/5.9$ for G2 and G10 in duplex (**2**).

[d]Coupling constant does not exist.

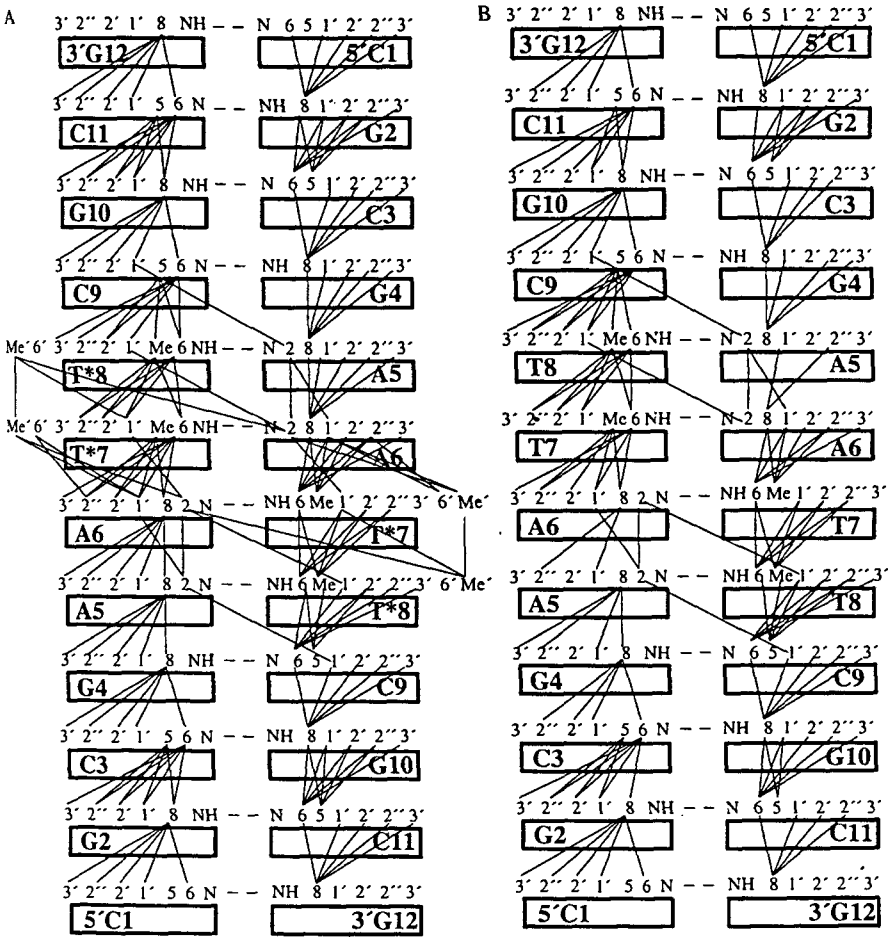

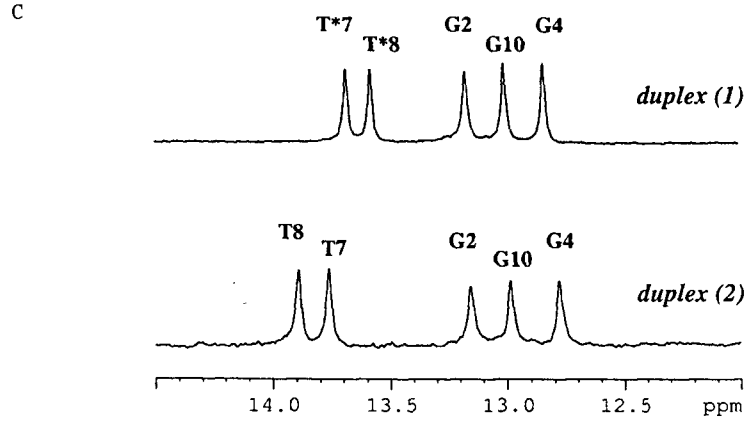

Figure 3: Schematic views of the interresidue distance constraints, based on NOESY experiments, used in the structure refinement of duplexes (**1**) (panel **A**) and (**2**) (panel **B**). Panel **C** shows the comparison of 1D NMR spectra for exchangeable imino protons of duplexes (**1**) and (**2**) at 15°C.

The phase angles of pseudorotation (P) and the puckering amplitudes (Ψ) for sugar moieties were obtained from the PSEUROT program using vicinal coupling constants in each sugar ring (17-19). This program uses a linear relationship to translate endocyclic torsions to proton-proton torsions. Parameters for such a relationship was hitherto unavailable for carbocyclic nucleosides. Hence, we have performed a series of *ab initio* (HF/6-31G*) calculations to derive these parameters, just in the same way as we performed earlier for 4′-thionucleosides (20). The set of 12 *ab initio* calculations was carried out by fixing the torsions ν_0 and ν_4 in such a way that the puckering amplitude in all starting structures was 45°, while the phase angle of pseudorotation (P) was incremented in 30° steps from 0° to 330°. The seven proton-proton torsions $\phi_{1'6'}$, $\phi_{1'2'}$, $\phi_{1'2''}$, $\phi_{2'3'}$, $\phi_{2''3'}$, $\phi_{3'4'}$, $\phi_{4'6'}$ and the three endocyclic torsions ν_1, ν_2 and ν_3 were obtained from the resulting energy-optimized structures. The resulting linear equations (Figure 5A) are as follows: $\phi_{1'6'} = -126.9+1.054\nu_0$, $\phi_{1'2'} = 122.2+1.091\nu_1$, $\phi_{1'2''} = 1.8+1.060\nu_1$, $\phi_{2'3'} = 2.9+1.126\nu_2$, $\phi_{2''3'} = 122.1+1.115\nu_2$, $\phi_{3'4'} = -125.1+1.088\nu_3$ and $\phi_{4'6'} = 129.1+1.032\nu_4$. These the-

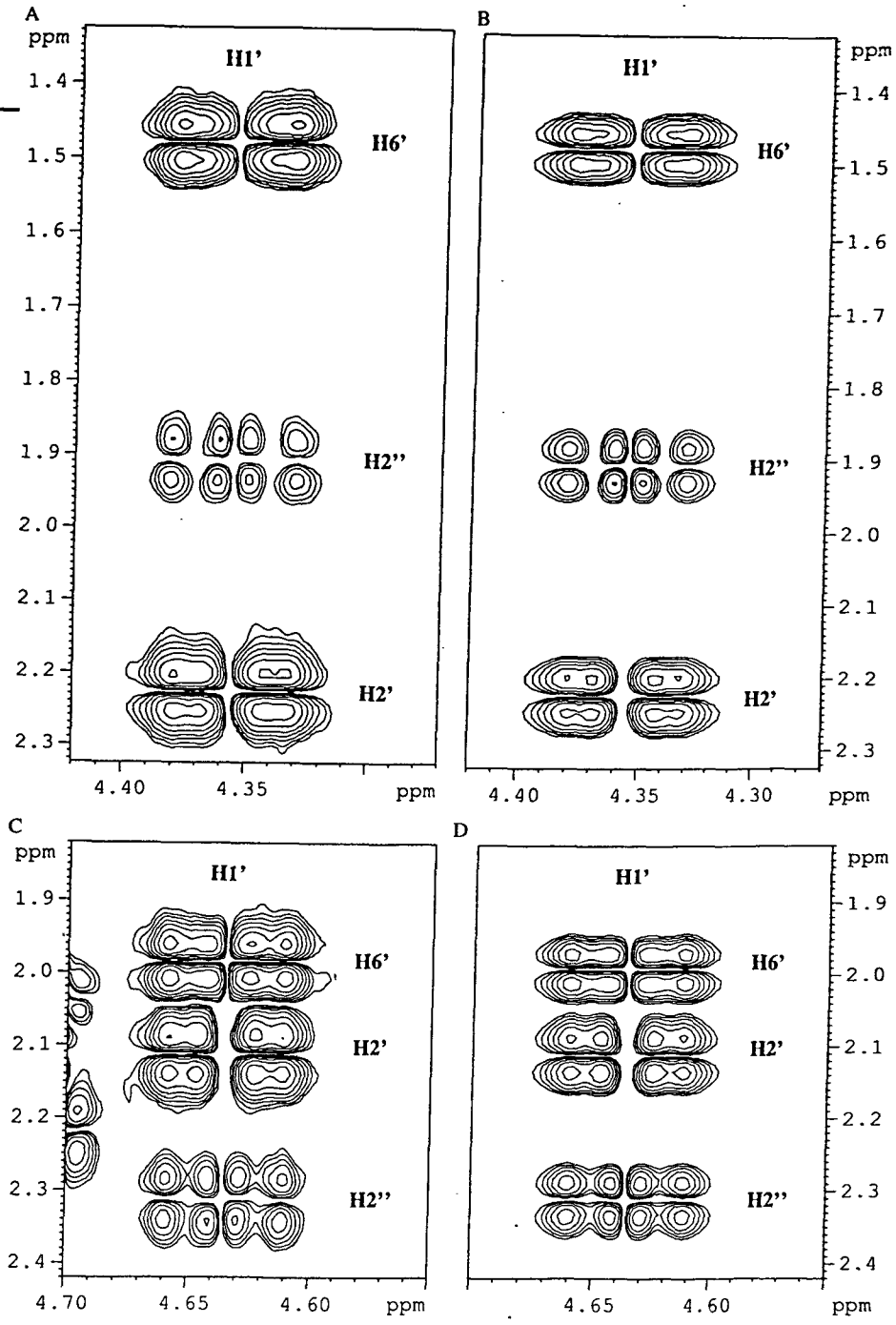

Figure 4: Expanded plots of DQF-COSY spectra (600 MHz) for duplex (**1**) at 20°C. Experimental (panels **A** and **C**) and best-fit simulated (using of the *NMRSIM* program) spectra (panels **B** and **D**) are presented for H1′-H2′/H2″/H6′ crosspeaks of T*7 (panels **A** and **B**) and T*8 (panels **C** and **D**) residues.

oretical investigations also showed that the 6′-α-Me carbocyclic thymidine pucker has two low-energy minima near P = 180° (South range) and near P = 60° (North-East range) with 1 kcal/mol energy preference for the former (Figure 5B). Running PSEUROT with the seven experimental $^3J_{HH}$ coupling constants for carbocyclic thymidines and the above parametrization gave us the P_S and Ψ_S values of sugar puckers in the C1′-*exo* range that are practically the same as for the unmodified thymidines as seen in Table II. This is also consistent with the X-ray crystal structures (2,21) for carbocyclic thymidine moieties in duplex (**1**) and the natural counterpart in duplex (**2**).

It was found that for the major conformer (>88%) P_S varies between 133° and 164°, while Ψ_S varies between 32° and 43° for practically all sugar and carbocyclic residues in both duplexes (**1**) and (**2**) (the minor conformer has not been modelled in this work). During DNA structure refinement, the geometry of the sugar rings were kept near the experimentally (using NMR-PSEUROT) determined P- and Ψ-

values by constraining the endocyclic ν_3 and ν_4 torsions calculated from the P and Ψ values (Table II) with a flat bottom harmonic potential. The ν_3 and ν_4 torsions were allowed to vary ±7° to take into account the errors in $^3J_{HH}$ coupling constants.

All sugar ring coupling constants could not be extracted for residues G2 and G10 in duplex (**2**) but we observed more than 90% of South-type conformation(16) for these residues (Table II) and have therefore constrained their sugars to P = 148°±15° and Ψ = 38°±6° in our molecular modeling.

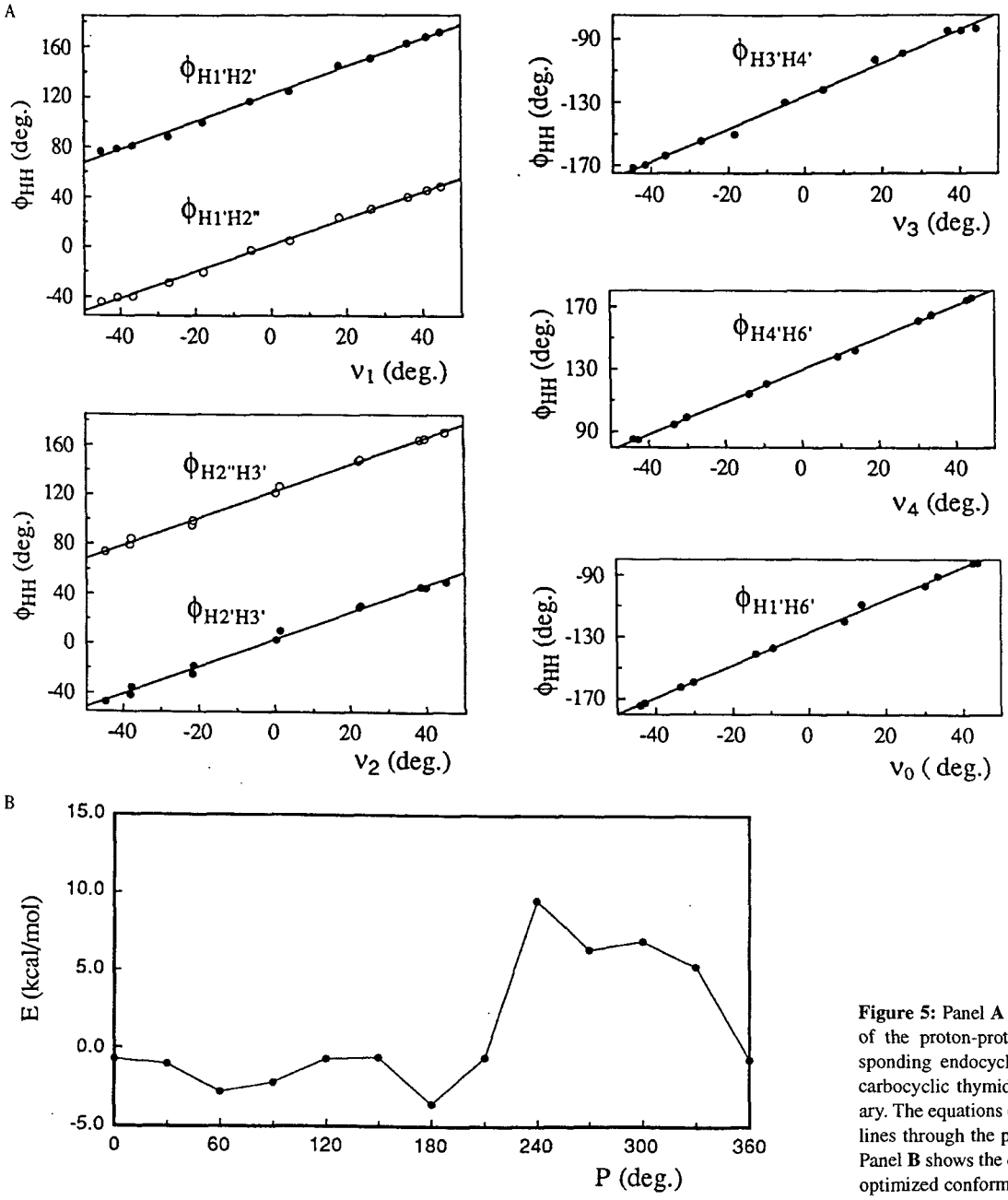

Figure 5: Panel **A** shows the calculated dependency of the proton-proton torsion angles on the corresponding endocyclic torsion angles (ν_0-ν_4) for the carbocyclic thymidine on the pseudorotation itinerary. The equations of the least-square best-fit straight lines through the points are summarized in the text. Panel **B** shows the dependency of the energy of these optimized conformers on the phase angles.

(C) Backbone β, γ and ε Torsions

(i) β torsions: Initially, the β torsion angles were estimated using the linewidths of NOESY crosspeaks of H6/H8 to H5′/H5″ in accordance with a literature procedure (22). Since these linewidths were found to be less than 28 Hz including the natural linewidth (4-6 Hz), we considered β to be 180°±75°. In order to confirm this preliminary qualitative conformational hyperspace for β, we performed H,C-correlation experiments for the determination of the vicinal $^3J_{C4'-P}$ coupling constants (23)

which gave us a more precise estimation of the β torsion. Unfortunately, the $^3J_{C4'-P}$ values for both 3′- and 5′-phosphates were very similar, hence we could only get the sums of $^3J_{C4'-P5'}$ and $^3J_{C4'-P3'}$ coupling constants for each unmodified nucleotide (21-24 Hz). For carbocyclic T*7 and T*8 thymidines, the sums of $^3J_{C4'-P5'}$ and $^3J_{C4'-P3'}$ coupling constants were less than 15 Hz, which is apparently more difficult to use because of the change of α-substituent effect from O4′ to the 6′-methine group in

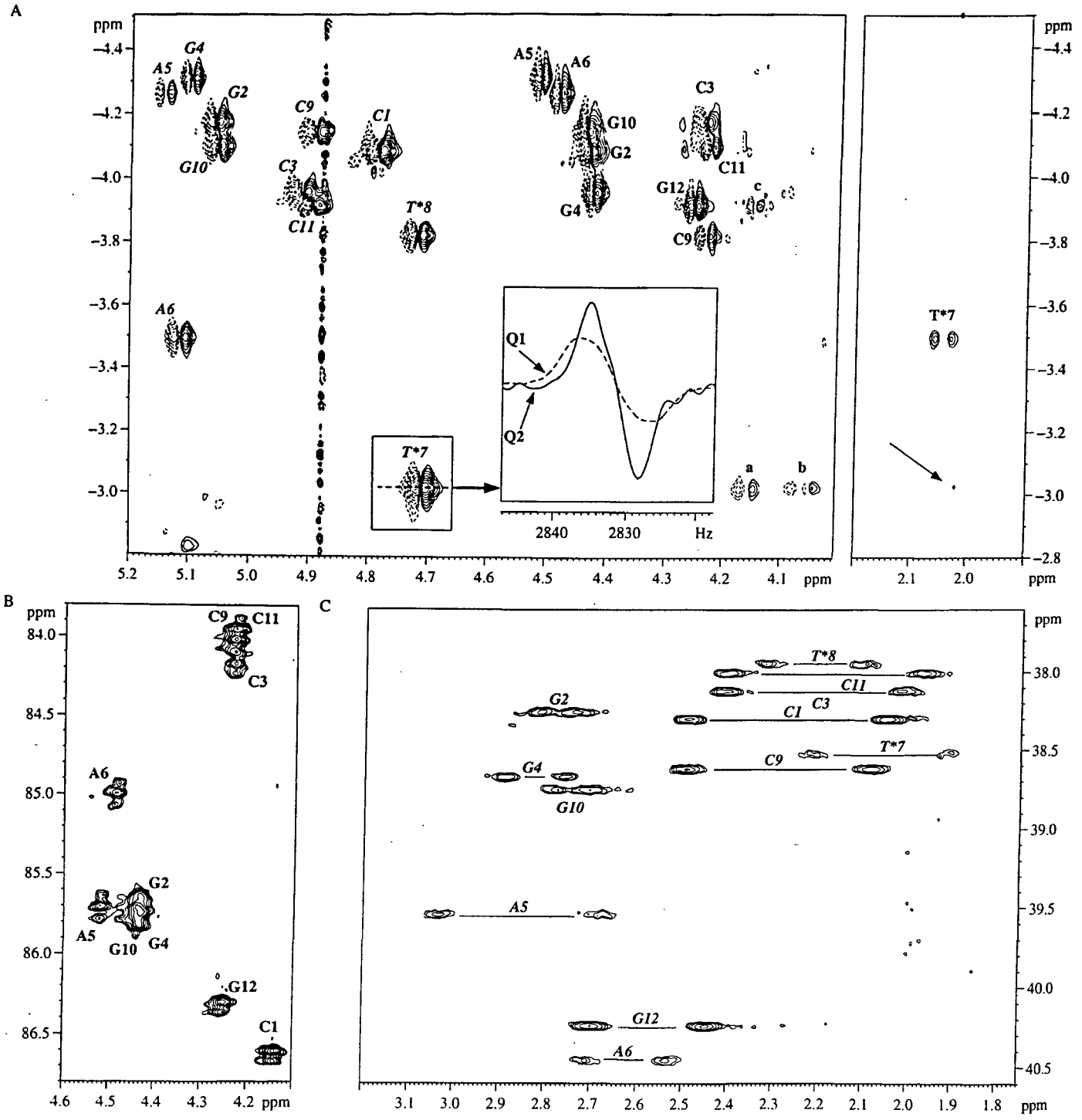

Figure 6: Panels **A**, **B** and **C** show expanded plots of H,P-correlation and one-bond H,C-correlation (HSQC) spectra (at 600 MHz for protons) for duplex (**1**) at 20°C. In panel **A**, the H3′-P$^{(3')}$ crosspeaks are labeled by the residue name and number (italic font), the H4′-P$^{(5')}$ crosspeaks are marked by the residue name and number (plain font) and the letters correspond to crosspeaks H5′/H5′-P$^{(5')}$ for T*8 (**a**, **b**) and G12 (**c**). The small arrow indicates the low intensity H4′-P$^{(5')}$ crosspeak (at d2.0 & d-3.0) for T*8. The positive component of the crosspeaks are shown by dashed line and the negative component by the solid line. The box in panel A shows two projections through T*7 crosspeak, one for experiment with double-homonuclear decoupled (at H2′, H2″ and H4′) showing (Q2) the enhancement of intensity because of elimination of the passive coupling, and the other without the homo decoupling showing (Q1) broadened peak from which no coupling constant can be derived. In panel **B**, the crosspeaks C4′-H4′ are labeled by the residue name and number. In panel **C**, the crosspeaks C2′-H2′ and C2′-H2″ are connected by solid lines and are labeled by the residue name and number.

the carbocyclic moieties. Taking the ^{13}C natural linewidth (4 Hz) of the unmodified nucleotide moieties into account, we could estimate values of $^3J_{C4'-P}$ constants for unmodified nucleotides to be 8 Hz as a lower limit, and therefore, we finally constrained the β torsions to 180°±40° using a flat bottom harmonic potential. The β torsions were derived using Karplus equation modified by Plavec *et al.* (24) and Lankhorst *et al.* (25). Individual $^3J_{C4'-P5'}$ coupling constants could however be obtained for terminal C1 (10.2 Hz) and G12 (9.8 Hz) residues.

Data for the β torsion angle in the carbocyclic residues was obtained through the H,P-correlation experiment (Figure 6A). We observed strong crosspeaks between H4′ and $P^{(5')}$ for all nucleotide residues, except for the T*8 residue, suggesting a four-bond W-type (26, 27) coupling pathway for H4′ and $P^{(5')}$, which means that H4′, C4′, C5′, O5′ and $P^{(5')}$ for all residues are coplanar except for those of the T*8 residue. It is likely that we do not see the crosspeak for the T*8 residue because the intensity of the crosspeak in our H,P-correlation experiment (Figure 6A) depends on two factors: (i) During the first INEPT step of the pulse sequence, the polarisation transfer is less effective due to small $^4J_{H4'-P}$ coupling constant, which decreases the intensity of the crosspeak (27). (ii) It is also conceivable that there is a cancellation of the intensity because the linewidth of the phase and antiphase components are broader than the actual coupling constant. This means (28) that the β torsion for T*8 residue is out of the usual range of 180°±40°. Strong H5′/H5″-$P^{(5')}$ crosspeaks (with more than 8 Hz of vicinal J_{HP} constant for the upfield H5′/H5″ proton, Figure 6A) were detected for T*8 residue that also indicates (22) that the β torsion for T*8 is not in the usual B-DNA range of 180°±40°.

Two flat bottom harmonic potentials were used for the β(T*8) torsional constraints to allow two different regions (105-135° and 225-255°, see Table III). Initially, small energy barriers separated the two allowed ranges (3-5 kcal/mol). The barrier heights were increased in later cycles of the MD-refinement.

Table III

NMR-based backbone torsion angle constraints (°) and the width of the flat bottom (in°) of the constraining harmonic potential used in minimization and MD calculations.

Residue	Duplex (1)			Duplex (2)		
	β	γ	ε	β	γ	ε
C1	-	-	170 ± 40	-	-	170 ± 40
G2	180 ± 40	60 ± 40	170 ± 40	180 ± 40	60 ± 40	170 ± 40
C3	180 ± 40	60 ± 15	170 ± 40	180 ± 40	60 ± 40	170 ± 40
G4	180 ± 40	60 ± 15	170 ± 40	180 ± 40	60 ± 40	170 ± 40
A5	180 ± 40	60 ± 15	170 ± 40	180 ± 40	60 ± 15	170 ± 40
A6	180 ± 40	60 ± 15	170 ± 40	180 ± 40	60 ± 15	170 ± 40
T*7/T7	180 ± 40	60 ± 15	170 ± 40	180 ± 40	60 ± 15	170 ± 40
T*8/T8	105-135, 225-255	60 ± 15	170 ± 40	180 ± 40	60 ± 15	170 ± 40
C9	180 ± 40	60 ± 15	170 ± 40	180 ± 40	60 ± 15	170 ± 40
G10	180 ± 40	60 ± 40	170 ± 40	180 ± 40	60 ± 40	170 ± 40
C11	180 ± 40	60 ± 40	170 ± 40	180 ± 40	60 ± 40	170 ± 40
G12	180 ± 40	60 ± 15	-	180 ± 40	60 ± 15	-

(ii) γ torsions: Constraints for the γ torsion angles were derived from the sum of the $J_{H4'-H5'}$ and $J_{H4'-H5''}$ coupling constants (22), which were available from $\Sigma_{4'}$ of sugar ring coupling constants in phosphorus decoupled DQF-COSY spectra (Table II), or from NOESY crosspeak linewidths of the H6/H8-H4′ together with comparing NOESY volumes between H6/H8 - H5′/H5″ and H6/H8-H1′ crosspeaks (22). The $\Sigma_{4'}$ of sugar ring coupling constants were less than 4 Hz for all nucleotide residues (except for the terminal C1 residue) which is consistent with a γ range of 60°±15°. For residues in which $\Sigma_{4'}$ of sugar ring coupling constants could not be used (G2, G10, C11 in duplex (**1**), and G2, C3, G4, G10 and C11 in duplex (**2**), see Tables II and III), we have used the linewidths of aromatics to H4′ (10-13 Hz), as well as the volumes of H6/H8-H5′/H5″ crosspeaks, which are smaller than the volumes of H6/H8-H1′ for NOESY spectra at 150 ms mixing time (Figure 2). This allowed us to put constraints for the g torsion angles to 60°±40° (flat bottom harmonic potentials).

(iii) ε torsions: The ε torsion angles have been measured from the vicinal $^3J_{H3'-P}$ coupling constants (29) (Table II), which lie in the range of 2-6 Hz. These values of coupling constants were determined from the comparison of H3′-H4′ crosspeak splittings in DQF-COSY spectra with and without phosphorus decoupling. We have also extracted $^3J_{H3'-P}$ from H,P correlation experiment by the removal of the passive coupling constant by double homonuclear decoupling, which are consistent with the range of $^3J_{H3'-P}$ from 2-6 Hz. These values of $^3J_{H3'-P}$ allowed us to constrain the ε torsions to 170°±40° (flat bottom harmonic potentials) consistent with B_I-type phosphate conformation (15,22). The B_I-type phosphate conformation was also verified by the measurement of $^3J_{C2'-P}$ vicinal coupling constants in the H,C-correlation spectra (Figure 6C), which was found to be close to zero Hz for all residues. Assuming $^3J_{C2'-P}$ is near 1 Hz (which is impossible to estimate within the error limit of our correlation experiments because of interference with the passive coupling constants of $^2J_{H2',H2''}$ as well as natural linewidth problem) for B_I-type and near 10 Hz for B_{II}-type (30), our experimental values suggest a clear preference for the B_I-type conformation for all nucleotide residues. In Figure 6B, we show the region of $^3J_{C4'-P}$ coupling constants in the H,C-correlation spectra for comparison with that of $^3J_{C2'-P}$ region (Figure 6c), showing that the $^3J_{C4'-P}$ coupling constants are indeed non-zero (~4-10 Hz), wheras the latter is very close to zero. It is noteworthy that ^{31}P signals for T*7, T*8 and C-9 of duplex (**1**) are shifted downfield by 0.5-1.3 ppm (Table II), which suggests (26) a B_{II}-type conformation for these residues, but our $^3J_{C2'-P}$ coupling constant measurement in fact contradicts this. The backbone torsion constraints are summarized in Table III.

(D) NMR Constraint Set

In order to find structures that are consistent with the experimental data, NMR-restrained molecular dynamics (MD) calculations were performed. The 474 NOE distance constraints (304 intra-, 164 interresidual and 6 interstrand) for duplex (**1**) and 390 NOE distance constraints (250 intra-, 136 interresidual and 4 interstrand) for duplex (**2**) were used (Figures 3A and 3B). They were generated by the complete relaxation matrix analysis using the RANDMARDI program (31,32). We also used 66 constraints for the β, γ and ε backbone torsion angles (Table III) and 48 constraints for endocyclic sugar torsion angles for both duplexes. It means that NMR structures have been based on 24 experimental distance and torsion constraints per residue for duplex (**1**) and 21 constraints per residue for duplex (**2**). Since we have observed the NMR signals for exchangeable imino protons (Figure 3C) involved in hydrogen bonds, we have also employed 32 distance constraints defining these Watson-Crick basepairing interactions. In addition, several torsional constraints ($\phi(C2^{Py}\text{-}N3^{Py}\text{-}N1^{Pu}\text{-}C6^{Pu})$ = 180°±20°, $\phi(C2^{Py}\text{-}C4^{Py}\text{-}N3^{Py}\text{-}N1^{Pu})$ = 180°±20° and $\phi(N3^{Py}\text{-}N1^{Pu}\text{-}C6^{Pu}\text{-}C2^{Pu})$ = 180°±20°) were used to ensure a reasonable degree of planarity within the basepairs (4, 33) due to the rather high temperatures (800 K) used during the MD simulations.

All experimental constraints were applied as flat bottom harmonic potentials with identical force constants for the lower bound and upper bound violations. The force constants employed for the constraint potentials were as follows: (i) All distance constraints (RANDMARDI derived and for Watson-Crick H-bonds) used 20 kcal.mol^{-1}.Å^{-2} in the initial cycles of MD-refinement and 30 kcal.mol^{-1}.Å^{-2} during later cycles. (ii) β, γ and ε backbone torsional constraints used 50 kcal.mol^{-1}.rad^{-2} during all five cycles. (iii) ν_3 and ν_4 sugar torsional constraints used 50 kcal.mol^{-1}.rad^{-2} during the initial cycles of MD-refinement and 100 kcal.mol^{-1}.rad^{-2} during later cycles. (iv) The torsional base-pair planarity constraints were only used during later stages of MD-refinement with 20 kcal.mol^{-1}.rad^{-2} force constants.

(E) Final Structures of MD/RANDMARDI Refinement

Canonical A- and B-type DNA conformers (Arnott coordinates from AMBER(34)) and X-ray structures (2,21) of both duplexes were used as the starting structures.

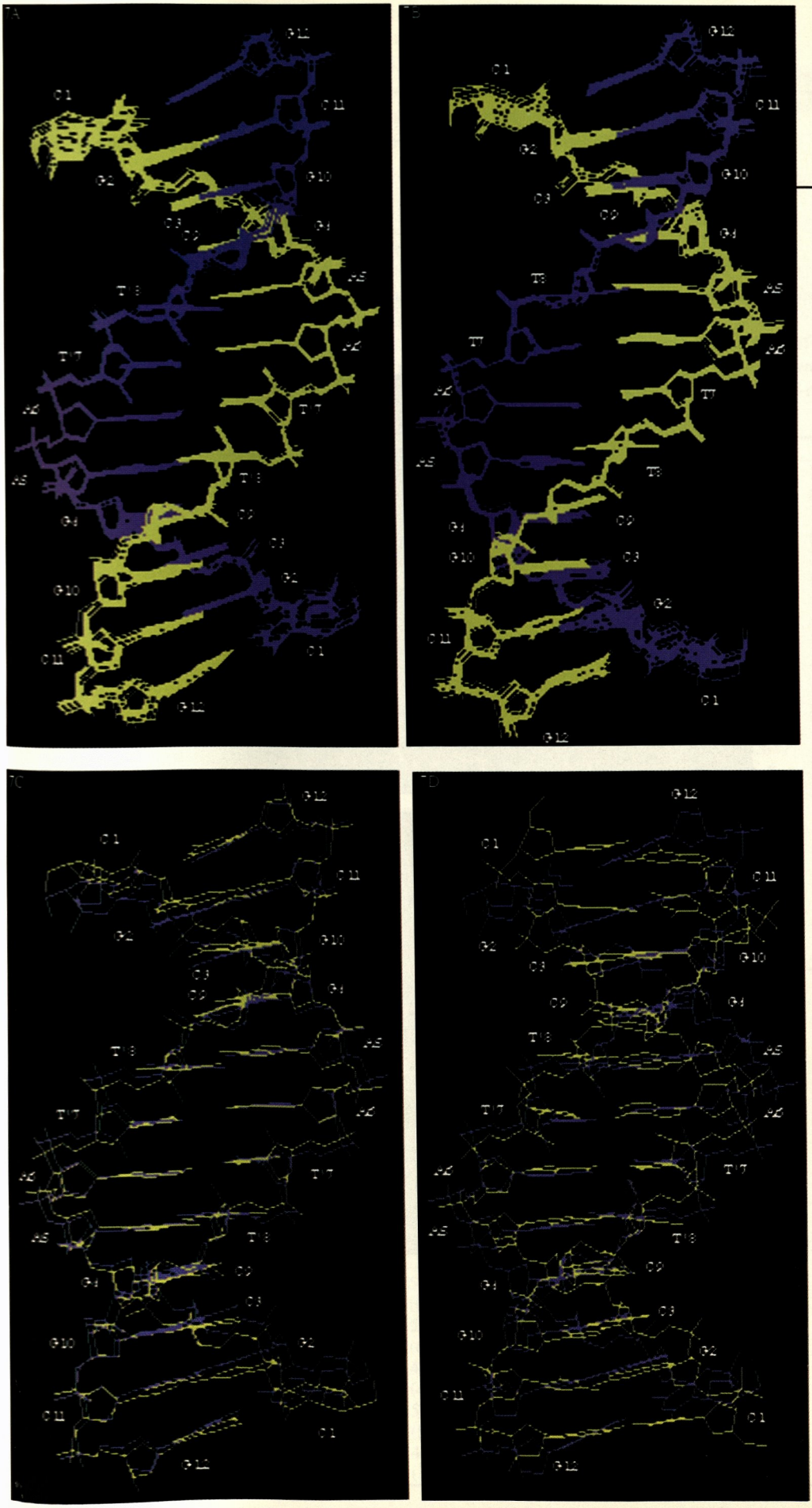

Figure 7: The superimpositions of the final nine individual structures (panels **A** and **B**) for duplexes (**1**) and (**2**). Panel **C** shows the superimposition of the final average structures of duplexes (**1**) (magenta) and (**2**) (yellow). Panel **D** shows the superimposition of the final average NMR structure (magenta) and the X-ray structure (yellow) of duplex (**1**). Figure 7 continued on the following page.

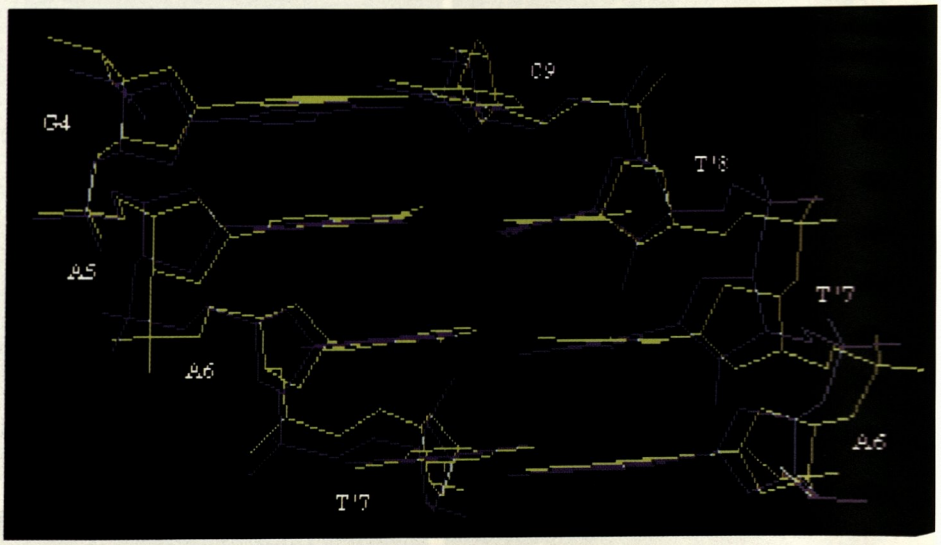

7E

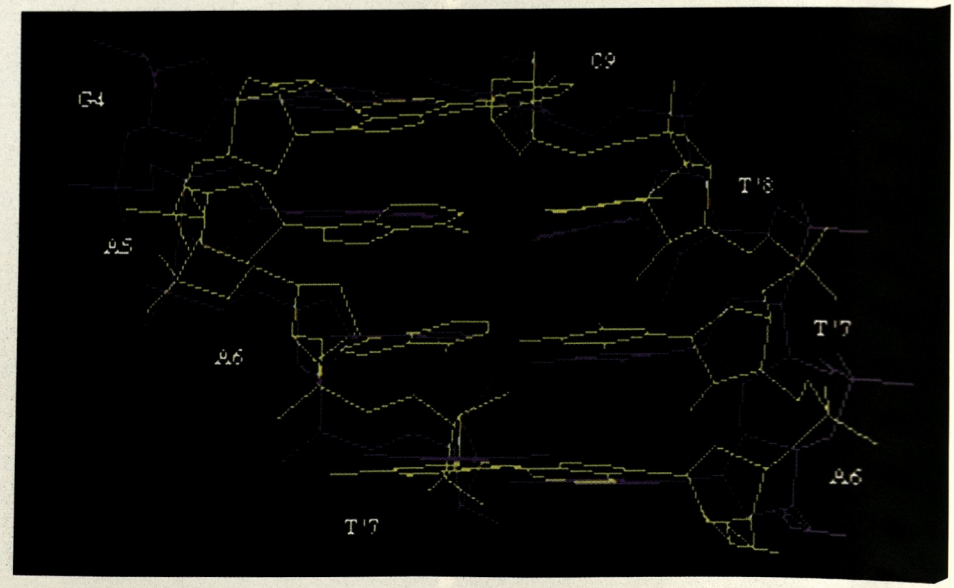

7F

Figure 7 Continued: An expanded part of panel **C** is shown in panel **E**, and an expanded part of panel **D** is shown in panel **F**.

Their atomic RMSD (for all heavy atoms) before the MD/RANDMARDI refinement procedure were 6.2Å between A- and B-type DNA, 1.3-1.4Å between B-type DNA and the respective X-ray structure, and 5.8-6.0Å between A-type and the corresponding X-ray structure. For both natural and modified duplexes, three separate calculations were carried out from each of the three starting structures, by using different random number seeds for the assignments of the initial velocities in MD calculations (4).

All nine final individual structures for duplex (**1**) were converged to an RMSD of 0.23-0.56Å. These nine structures are superimposed in Figure 7, and the ranges of

Table IV

The ranges of torsion angles and phase angles of pseudorotation (P) for the final individual NMR structures[a] and X-ray structures (in parenthesis)[b] of duplexes (**1**) and (**2**).

[a]All 9 final individual NMR structures of duplexes (**1**) and (**2**) were used for determination of ranges of torsions and phase angles in both strands. The central values of these ranges with corresponding deviations are shown.

[b]The X-ray structure parameters in the parenthesis are for first and second strands, respectively. The X-ray structures with codes BDL001 and BDLS79 were taken from NDB (see text).

Duplex	Residue	α	β	γ	ε	ζ	χ	P
(1)	C1	-	-	-	205 ± 4	281 ± 3	234 ± 6	127 ± 4
		-	-	-	(220, 209)	(181, 204)	(251, 275)	(141, 189)
(1)	G2	280 ± 5	180 ± 5	49 ± 4	182 ± 8	257 ± 9	258 ± 4	156 ± 4
		(34, 298)	(140, 159)	(211, 46)	(193, 194)	(221, 234)	(280, 258)	(193, 152)
(1)	C3	287 ± 3	176 ± 3	61 ± 4	187 ± 2	277 ± 2	238 ± 3	129 ± 2
		(309, 301)	(150, 145)	(54, 65)	(182, 189)	(263, 281)	(223, 221)	(109, 45)
(1)	G4	292 ± 3	175 ± 2	45 ± 2	181 ± 4	253 ± 4	251 ± 3	155 ± 1
		(280, 280)	(194, 189)	(66, 72)	(161, 181)	(265, 255)	(254, 260)	(147, 159)
(1)	A5	289 ± 3	188 ± 2	53 ± 1	185 ± 2	269 ± 2	238 ± 3	150 ± 2
		(289, 286)	(204, 188)	(58, 56)	(185, 198)	(257, 263)	(262, 254)	(172, 175)
(1)	A6	287 ± 3	179 ± 3	56 ± 2	192 ± 2	255 ± 4	243 ± 3	141 ± 2
		(289, 289)	(186, 188)	(51, 44)	(215, 189)	(225, 255)	(265, 260)	(163, 161)
(1)	T*7	286 ± 3	170 ± 2	57 ± 2	211 ± 2	224 ± 7	239 ± 6	138 ± 4
		(299, 286)	(153, 168)	(43, 49)	(249, 257)	(189, 189)	(274, 261)	(147, 154)
(1)	T*8	310 ± 5	136 ± 2	59 ± 2	189 ± 3	273 ± 3	231 ± 6	132 ± 8
		(277, 283)	(157, 140)	(45, 49)	(323, 140)	(105, 299)	(257, 239)	(142, 111)
(1)	C9	293 ± 5	184 ± 2	53 ± 3	188 ± 3	274 ± 4	225 ± 5	143 ± 6
		(195, 271)	(211, 216)	(61, 57)	(73, 194)	(76, 266)	(229, 268)	(16, 164)
(1)	G10	286 ± 4	185 ± 3	39 ± 4	181 ± 5	255 ± 7	251 ± 5	150 ± 2
		(229, 290)	(160, 176)	(61, 51)	(250, 199)	(178, 210)	(258, 281)	(164, 152)
(1)	C11	293 ± 4	182 ± 3	56 ± 2	184 ± 3	276 ± 3	225 ± 5	140 ± 5
		(292, 310)	(156, 142)	(49, 49)	(174, 180)	(278, 285)	(263, 223)	(176, 65)
(1)	G12	295 ± 3	176 ± 4	57 ± 3	-	-	246 ± 6	139 ± 4
		(264, 274)	(190, 174)	(59, 57)	-	-	(259, 220)	(101, 31)
(2)	C1	-	-	-	195 ± 3	287 ± 3	233 ± 6	122 ± 3
		-	-	-	(219, 201)	(216, 235)	(255, 232)	(161, 153)
(2)	G2	275 ± 5	175 ± 3	38 ± 4	180 ± 7	249 ± 9	256 ± 5	143 ± 7
		(294, 309)	(170, 164)	(40, 49)	(174, 178)	(262, 267)	(249, 244)	(140, 128)
(2)	C3	295 ± 2	177 ± 4	64 ± 5	187 ± 2	274 ± 3	235 ± 3	142 ± 2
		(297, 297)	(172, 169)	(59, 60)	(183, 175)	(272, 274)	(225, 226)	(93, 68)
(2)	G4	283 ± 3	181 ± 3	45 ± 4	182 ± 8	251 ± 9	250 ± 4	146 ± 2
		(297, 291)	(181, 171)	(57, 73)	(205, 174)	(207, 262)	(267, 245)	(166, 149)
(2)	A5	293 ± 2	186 ± 4	52 ± 3	182 ± 2	251 ± 4	243 ± 3	150 ± 3
		(317, 303)	(143, 190)	(52, 54)	(180, 177)	(268, 263)	(234, 254)	(129, 169)
(2)	A6	293 ± 3	183 ± 2	55 ± 3	188 ± 3	267 ± 7	242 ± 4	148 ± 4
		(287, 303)	(180, 186)	(66, 48)	(174, 174)	(272, 259)	(238, 252)	(127, 147)
(2)	T7	291 ± 4	174 ± 6	59 ± 6	186 ± 3	275 ± 2	225 ± 2	120 ± 1
		(303, 302)	(181, 174)	(52, 60)	(174, 179)	(274, 272)	(233, 229)	(101, 116)
(2)	T8	296 ± 2	174 ± 2	56 ± 3	184 ± 2	271 ± 2	221 ± 3	131 ± 2
		(301, 301)	(173, 179)	(64, 55)	(171, 179)	(271, 266)	(234, 240)	(116, 130)
(2)	C9	290 ± 2	185 ± 3	57 ± 3	183 ± 3	272 ± 4	230 ± 3	138 ± 6
		(301, 301)	(181, 185)	(61, 45)	(203, 183)	(266, 274)	(240, 246)	(140, 114)
(2)	G10	289 ± 3	182 ± 4	45 ± 3	188 ± 4	248 ± 6	246 ± 4	146 ± 3
		(293, 293)	(169, 179)	(47, 50)	(257, 260)	(150, 172)	(270, 272)	(146, 156)
(2)	C11	291 ± 3	182 ± 3	56 ± 3	184 ± 2	273 ± 2	243 ± 4	141 ± 2
		(286, 288)	(139, 139)	(56, 45)	(198, 186)	(270, 263)	(235, 235)	(147, 117)
(2)	G12	284 ± 4	179 ± 2	45 ± 2	-	-	250 ± 5	136 ± 1
		(279, 295)	(176, 171)	(57, 47)	-	-	(248, 225)	(114, 35)

their torsion angles and sugar puckers are presented in Table IV. The final 9 individual structures are similar both in terms of potential energy (373±7 kcal/mol) and different R-factors(35): R = 0.314±0.005; R_2 = 0.396±0.004; R^x = 0.056±0.001; R^x_2 = 0.067±0.001 for NOESY at 150 ms. These final nine individual structures were superimposed, averaged, symmetrized and energy minimized using the combined average distance constraints obtained from RANDMARDI calculations to give the final average structure for duplex (**1**). The same set of combined average distance constraints was used for both strands for maintaining the 2-fold symmetry of the duplex because we obtained only one set of NMR signals. The RMSD of the average structure of duplex (**1**) with all 9 final individual structures varies from 0.22 to 0.37Å. The same procedure gave us the final average structure for duplex (**2**). The individual 9 final structures for duplex (**2**) are similar both in terms of potential energy (357±6 kcal/mol) and R-factor analyses for 150 ms NOESY: R = 0.294±0.005; R_2 = 0.324±0.006; R^x = 0.053±0.001; R^x_2 = 0.063±0.001. The RMSD values for these 9 individual final structures of duplex (**2**) are in range of 0.19-0.55Å (Figure 7), and RMSD of the final average structure of duplex (**2**) with 9 final individual structures were 0.23-0.48Å. The atom coordinates of final average structures are deposited to the Protein Data Bank (PDB, Brookhaven National Laboratory), and these NMR structures are shown in Figure 7. The PDB identification codes are 1DAU and 2DAU for duplexes (**1**) and (**2**), respectively.

(F) Structural Analysis and Features

(i) Comparison with Previous NMR Sructures

The RMSD for all heavy atom comparison of the final average structure for duplex (**1**) with canonical A- and B-type DNA gave values of 4.43Å and 3.06Å, respectively, whereas a similar comparison with duplex (**2**) gave the corresponding values of RMSD of 4.76Å and 3.40Å. The RMSD of our final average structure of natural duplex (**2**) with an earlier NMR structure (4) of this duplex (code 171D at Brookhaven PDB) is 1.72 Å, but the main difference between our structure and the previous structure is probably due to the absence of appropriate constraints for the γ torsion angles in the latter. As a result, the NMR structure (4) has γ(A6) = 101° and γ(T7) = 2°, which do not agree with our experimental data (Table III). The atomic coordinates of other NMR structures (9,10) of Dickerson-Drew duplex (**2**) are not presented in the Brookhaven PDB, but analysis of literature data showed that experiments were carried out at different conditions (for example, our salt concentration is ten times higher than in the study of Nerdal *et al.* (9) and the molecular modeling was made without backbone torsion constraints from the NMR data (10)). Nevertheless, some general features of our NMR structures were consistent with those of the literature NMR structures: The twist between C3:G10 and G4:C9 or between central A6:T7 and T7:A6 basepairs (Figure 8) decreased due to the interstrand steric hindrance between purines (36,37).

(ii) Comparative Analysis of Present NMR Structures

The RMSD for all heavy atoms between our structures for duplexes (**1**) and (**2**) is 1.02Å, whereas exclusion of the terminal C1 and G12 residues gives an RMSD of 0.90Å. The distances between 7′-carbon atoms of methyl groups within the strand in duplex (**1**) are 5.2Å, and they are 5.6Å for the opposite strands. Detailed comparison of the backbone torsion angles, sugar puckers, minor groove widths (38) and helical (local Cartesian) structure parameters (39) of final average structures of duplexes (**1**) and (**2**) are given in Figure 8 and Table V. The most significant differences (27-50°) between backbone torsions were found for the β torsion of T*8 in duplex (**1**) with T8 of duplex (**2**) and for the ε, ξ torsions of T*7 in duplex (**1**) with T7 of duplex (**2**), which are located at the site of duplex modification. Nevertheless, the helical structure parameters (Table V) have relatively small deviations for conformations of duplexes (**1**) and (**2**), giving a structural isomorphism in aqueous solution. The basepair twist increased by 6° for the 4-5 and 8-9 basepair steps (*i.e.*

between T*8:A5 and C9:G4 basepairs) and it decreased by 5° for the 5-6 and 7-8 steps (T*7:A6 to T*8:A5) for the modified duplex with respect to the native duplex. Some differences between the helical parameters in the core parts of the NMR duplexes (Table V) were also found for the basepair tilts for the 4-5 and 8-9 steps (7°), basepair rolls for the 5-6 and 7-8 steps (7°), basepair shifts for the 5-6 and 7-8 steps (0.9Å) and basepair slides for the 3-4 and 9-10 steps (0.6Å). The basepair rises are very similar for both duplex structures. Deviations for helical parameters involving the T*8 base can be more significant due to the fact that the pyrimidine-pyrimidine 7-8 and 8-9 base steps show virtually no intrastrand base-base overlap whereas the purine-purine and purine-pyrimidine steps exhibit a modest degree of intrastrand base-base overlap (4).

The difference of the minor groove widths in the core part of the modified duplex in comparison with the native one is much smaller between the NMR structures (less than 0.7Å, Figure 8) than between the X-ray structures of these duplexes (2.3Å on average(2)). It is noteworthy that recently published theoretical calculations (40) of duplex (2) showed deviations of minor groove widths of more than 2Å during a 1 ns molecular dynamics simulation. The weaker thermal stability (T_m is

Figure 8: The panels show the backbone torsion angles (α, β, γ, ε, ζ), the glycosidic torsion angle (χ), the phase angle of pseudorotation (P) for each residue, the helical parameters for basepairs and the minor groove widths in the core part of the final average structures of duplexes (**1**) (filled circles) and duplex (**2**) (open circles). The minor groove width is defined as the shortest phosphorus-phosphorus interatomic distance across the groove less 5.8Å to compensate for the van der Waals radii of the two phosphate groups.

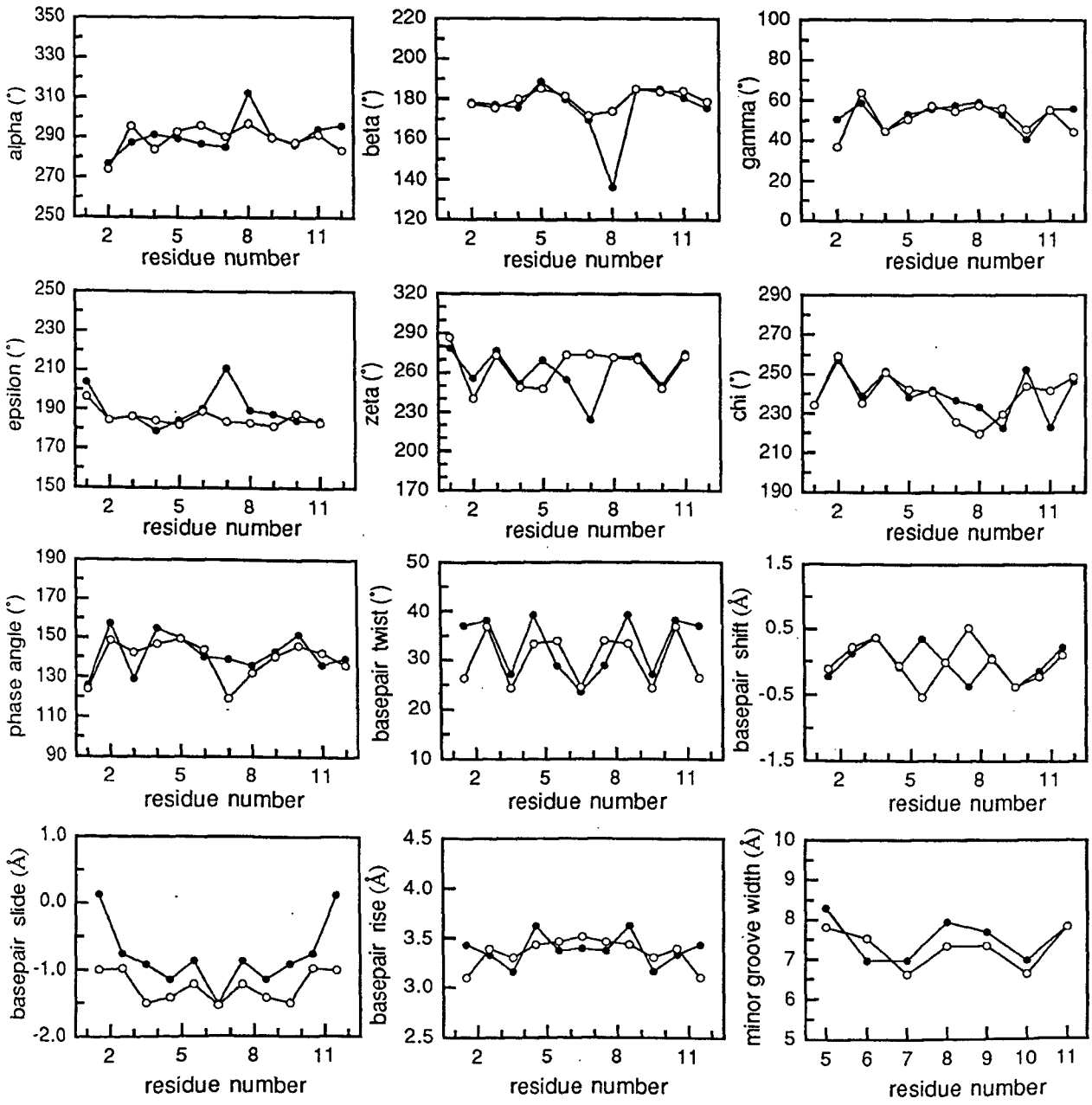

lowered by 3-4°) of the modified duplex (1) compared to duplex (2) is probably not due to the small changes of minor groove widths but due to the difference of duplex hydrations at the core part, *i.e.* the release of water molecules in the vicinity of the methyl substituents of the modified thymidine residues (2,41).

(iii) Detailed Comparison of NMR Structures with X-ray Structures

The discrepancy between NMR solution and crystallographic X-ray structures is well known in literature most probably as a result of crystal packing forces (4,9,10,42,43). The two strands are not identical (21,44) for crystal structures of duplexes (1) and (2) in contrary to the symmetrical NMR structures, which is evident by a single set of the NMR signals in the buffered aqueous solution (see experimentals). The most significant asymmetric geometrical changes in backbone conformation was found for ε and ξ torsions of duplex (1) probably due to the crystal packing forces (2). Thus, this crystal structure has ε(T*8) = 323° and ε(C9) = 73° for one strand whereas the same ε torsion angles for the second strand are equal to

Table V

Structure parameters for basepairs of final average NMR structures and X-ray structures of duplexes (1) and (2)[a].

Step	1st basepair	2nd basepair	Duplex	Type	Tilt	Roll	Twist	Shift	Slide	Rise
1-2	C:G	G:C	(1)	NMR	-10.7	12.1	37.0	-0.23	0.13	3.43
				X-ray	-1.0	3.6	39.6	-0.51	0.40	3.46
			(2)	NMR	-5.2	13.3	26.3	-0.11	-1.00	3.10
				X-ray	-3.5	6.1	42.6	-0.39	0.36	3.40
2-3	G:C	C:G	(1)	NMR	2.3	4.6	38.1	0.13	-0.76	3.33
				X-ray	-0.7	-0.5	39.3	0.19	0.24	3.52
			(2)	NMR	1.2	10.9	36.8	0.22	-0.98	3.39
				X-ray	1.0	-5.3	36.0	0.49	0.26	3.50
3-4	C:G	G:C	(1)	NMR	-1.5	1.1	27.1	0.38	-0.92	3.16
				X-ray	3.6	6.1	34.9	-0.15	0.96	3.50
			(2)	NMR	2.0	-3.9	24.3	0.37	-1.50	3.30
				X-ray	3.1	8.8	26.8	-0.33	0.83	3.27
4-5	G:C	A:T	(1)	NMR	9.0	8.9	39.2	-0.08	-1.15	3.62
				X-ray	-3.6	2.8	33.4	0.06	0.08	3.26
			(2)	NMR	2.2	9.9	33.3	-0.05	-1.42	3.43
				X-ray	-3.3	2.0	40.4	-0.06	0.12	3.29
5-6	A:T	A:T	(1)	NMR	-1.6	0.3	28.8	0.36	-0.87	3.37
				X-ray	-2.0	0.8	34.5	0.31	0.22	3.26
			(2)	NMR	-0.9	-6.2	33.9	-0.53	-1.22	3.46
				X-ray	-0.8	0.3	35.3	0.04	-0.32	3.29
6-7	A:T	T:A	(1)	NMR	0.0	2.4	23.5	0.00	-1.52	3.39
				X-ray	4.4	7.9	28.1	-0.12	-0.37	3.55
			(2)	NMR	0.0	2.2	24.5	0.00	-1.54	3.51
				X-ray	2.0	-3.6	33.6	0.31	-0.69	3.28
7-8	T:A	T:A	(1)	NMR	1.6	0.3	28.8	-0.36	-0.87	3.37
				X-ray	-1.7	5.7	35.8	-0.38	0.15	3.41
			(2)	NMR	0.9	-6.2	33.9	0.53	-1.22	3.46
				X-ray	3.2	-0.1	35.2	-0.16	-0.19	3.29
8-9	T:A	C:G	(1)	NMR	-9.0	8.9	39.2	0.08	-1.15	3.62
				X-ray	-2.4	-7.2	46.6	-0.19	0.10	3.36
			(2)	NMR	-2.2	9.9	33.3	0.05	-1.42	3.43
				X-ray	0.9	-0.9	39.0	0.07	-0.02	3.25
9-10	C:G	G:C	(1)	NMR	1.5	1.1	27.1	-0.38	-0.92	3.16
				X-ray	-2.5	7.6	28.6	0.51	0.80	3.31
			(2)	NMR	-2.0	-3.9	24.3	-0.37	-1.50	3.30
				X-ray	-2.8	4.6	31.7	0.38	0.97	3.42
10-11	G:C	C:G	(1)	NMR	-2.3	4.6	38.1	-0.13	-0.76	3.33
				X-ray	0.5	-14.0	43.2	-0.86	0.58	3.60
			(2)	NMR	-1.2	10.9	36.8	-0.22	-0.98	3.39
				X-ray	-5.2	-13.5	38.4	-1.27	0.39	3.64
11-12	C:G	G:C	(1)	NMR	10.7	12.1	37.0	0.23	0.13	3.43
				X-ray	6.9	1.2	32.9	0.84	0.81	3.60
			(2)	NMR	5.2	13.3	26.3	0.11	-1.00	3.10
				X-ray	3.3	-3.0	34.7	0.76	0.18	3.41

[a]Tilt, roll and twist are in degrees; shift, slide and rise are in Å (39). The X-ray structures with codes BDL001 and BDLS79 were taken from NDB (see text).

140° and 194° respectively (2).

The RMSD for all heavy atoms of our NMR structures from the X-ray structures (2,21) are 2.65Å and 3.28Å for duplexes (**1**) and (**2**) respectively. A detailed comparison of NMR and X-ray structure parameters are presented in Tables IV and V, Figures 9 and 10. Deviations of more than 100° were found for backbone torsions α,γ(C2), ε,ξ(T*8 and C9), phase angles P(C9 and G12 in different strands) in the modified duplex (**1**). The NMR and X-ray backbone torsion and phase angle parameters are closer to one another for the natural duplex (**2**), but some parameters such as ε,ξ(G10 in both strands) and P(C3 and G12 in second strand) have deviations in the range of 70-100°. Though these big deviations prevented us from more detailed analysis of backbone torsions, it is noteworthy that the β(T*8) torsions in duplex (**1**) are similar for the X-ray and NMR structures (Figure 9).

The analysis of helical parameters for basepairs (Table V) showed that the most significant differences between NMR and X-ray structures concern all basepair slides (0.9-2.5Å) in the core parts of both duplexes (Figures 9 and 10). These monotonic changes of the basepair slides can most probably be responsible for the decrease of

Figure 9: The comparison of the backbone torsion angles (α, β, γ, ε, ζ), the glycosidic torsion angle (χ), the phase angle of pseudorotation (P) for each residue, the helical parameters for basepairs and the minor groove widths in the core part of the final average NMR structure (solid lines) and the X-ray structure (dotted and dashed lines for first and second strands) of duplex (**1**).

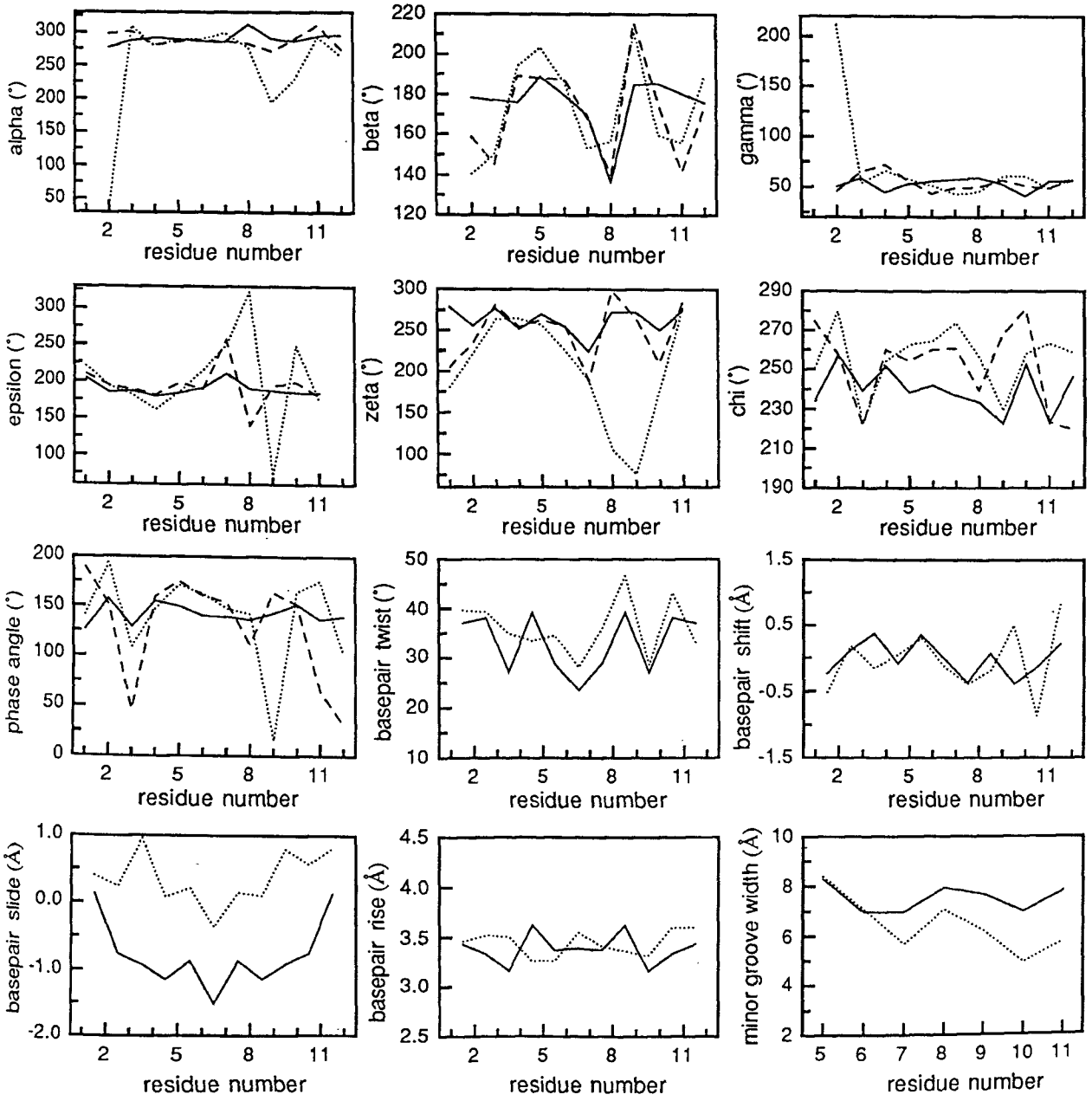

the minor groove widths of X-ray structures with respect to NMR structures (Figures 9 and 10) and the significant atomic RMSD between NMR and X-ray structures. It should be mentioned that the deviations in basepair slides were found earlier for other B-DNA duplexes: negative average slide values are encountered in the NMR structures, whereas positive average slide values were found for X-ray structures (43). Deviations between NMR and X-ray structure parameters were also found for the basepair tilt of the 4-5 step (13°), basepair rolls for the 8-9 and 10-11 steps (16° and 19°), basepair twist of the 3-4 step (8°), basepair shift of the 9-10 step (0.9Å) in the core part of duplex (**1**) and for basepair rolls for the 2-3 and 10-11 steps (16° and 23°), basepair twist of the 6-7 step (9°), basepair shift of the 10-11 step (1.1Å) in the core part of duplex (**2**). The deviations of basepair rises are small (less than 0.4Å) for both duplexes. The significant negative values (0.8-1.5Å) of basepair slides give both our NMR structures some features which are more typical for A-type DNA (33,43). Nevertheless, the other NMR structure parameters such as South-type sugar puckers or the backbone torsions (especially ξ = 224-287°) and the atomic RMSD between the A-type or the B-type DNA with the NMR structures for both duplexes (**1**) and (**2**) (see above) show strong structural similarity of the solution structures with that of the B-type.

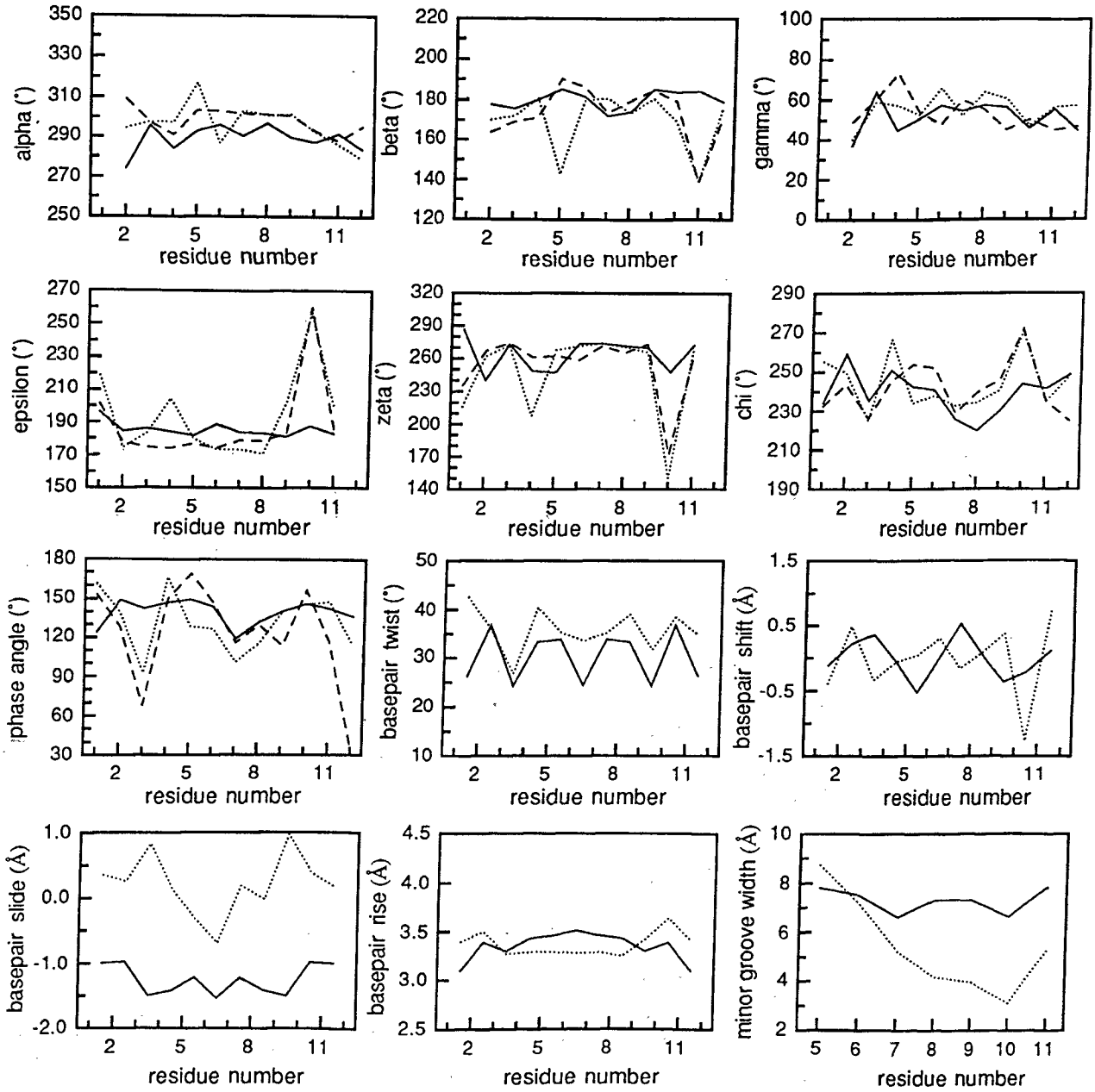

Figure 10: The comparison of structure parameters (as in Figure 9) of the final average NMR structure (solid lines) and the X-ray structure (dotted and dashed lines for first and second strands) of the natural duplex (**2**).

(iv) Comparative Thermodynamics of Duplexes (I) and (II)

The thermodynamics of the duplex (1) with hydrophobic 7′-α-methyl group of T_{Me} [$\Delta H° = -256 \pm 2$ kJ/mol, $-T\Delta S° = 198 \pm 2$ kJ/mol, $\Delta G°(298K) = -58 \pm 2$ kJ/mol] with respect to the natural Dickerson-Drew dodecamer [$\Delta H° = -343 \pm 3$ kJ/mol, $-T\Delta S° = 269 \pm 2$ kJ/mol, $\Delta G°(298K) = -74 \pm 3$ kJ/mol] are indeed very different under identical buffer condition (1M NaCl, 200 mM NaH_2PO_4, 10μM EDTA, pH 7.3). Although the structures of these two duplexes are very similar (r.m.s.d = 1Å), the $\Delta G°$ (and the contributing $\Delta H°$ and $-T\Delta S°$) of their thermodynamic stabilities are very different. The difference in the thermodynamics between duplexes (1) and (2) can be attributed due to the absence of stereoelectronic gauche and anomeric effects (8) (and the steric contribution of the methyl group) in the former compared to the latter. It is also likely that the net result of these counteracting effects [as well as the steric effect of 7′-α-methyl group in duplex (1)] may culminate into enhanced hydrophobic effect displacing water molecules from the minor groove in duplex (1) compared to duplex (2). Attempts are now being made to distinguish these stereoelectronic and steric effects (8) by comparison with an identical duplex but with 2′-deoxyaristeromycin instead of T_{Me}.

Conclusion

The NMR structure of the carbocyclic modified oligonucleotide has mixed features of both A- and B-type DNA, just as in the natural counterpart, but in general the solution conformations are more similar to B-type DNA. Replacement of the sugar oxygen O4′ by the C6′-carbon atom bearing an α-Me substituent does not considerably change the conformation of the modified DNA duplex compared to the natural counterpart in aqueous solution. This is because of the fact that the absence of the stereoelectronic anomeric and gauche effects in the carbocyclic moieties of the modified duplex allow them to take up the conformation of the natural furanose dictated by the neighbouring natural nucleotides. This makes the carbocyclic nucleotide an ideal mimic of the natural counterpart. The introduction of these carbocyclic moieties in the antisense DNA and RNA or in triplex DNA enhances the stabilities of these modified nucleic acids against nucleases. It is expected that these modified oligonucleotides will have improved lipophilicity, which may help their penetration inside the cell in the antisense and antigene therapy.

Materials and Methods

(i) Sample Preparation

Syntheses of modified thymidines and the d(CGCGAAT*T*CGCG) oligonucleotide containing these carbocyclic thymidines have been previously described (1,2). For NMR experiments, the oligonucleotides were purified additionally by successive passage through a column of Dowex 50 (Na^+) resin. The NMR samples (150 OD_{260} units) were twice lyophilized to dryness from D_2O and dissolved in 0.6 ml of the buffer (0.1 M NaCl, 10 μM NaH_2PO_4, 10 mM EDTA sodium salt, pH 7.4) in D_2O (99.96% D) or 9:1 H_2O/D_2O, v/v.

At UV concentration (1 μM per strand in the buffer: 0.1 M NaCl, 10 mM NaH_2PO_4, pH 7.3), the transition temperatures (T_m) for duplexes (**1**) and (**2**) are 44.1°C and 48.4°C. The difference between T_m values for duplexes (**1**) and (**2**) is very close to previously reported values (2).

For the calculations of $\Delta H°$, $\Delta S°$ and $\Delta G°$, T_ms at five different oligonucleotide concentrations (8,12,16,20, and 24 μM total single strand concentration) were measured.

(ii) NMR Spectroscopy

The NMR spectra were recorded on Bruker DRX-600 and DRX-500 spectrometers

operating at 600.13 and 500.13 MHz for protons. Phase-sensitive NOESY experiments in D_2O (with mixing times of 70, 150, 200 and 300 ms) at 20°C and in water-D_2O (9:1, v/v) with 160 ms mixing time at 5°C for both duplexes were performed giving final spectra with 2Kx2K data points after Fourier transformation. The volumes of all crosspeaks in the NOESY spectra were calculated using the AURELIA (v. 2.1, Bruker) program. The DQF-COSY spectra were collected with and without phosphorus decoupling giving final spectra of 8Kx1K. The COSY crosspeaks were simulated using the NMRSIM (v. 2.5, Bruker) program taking the relaxation properties of the sugar protons into account to accomodate the linewidth problem. The MLEV-17 HOHAHA experiment was recorded at a mixing time of 96 ms. Relaxation delay for all these experiments was 3 s, the number of experiments were 512 and the number of scans were 64 or 128 for each FID. The inverse H,C-correlation HSQC spectra were recorded with adjusting on $^1J_{CH}$ to 145 Hz and GARP sequence for heteronuclear decoupling, the number of experiments were 2K. The inverse H,P-correlation spectra (27) were measured with adjusting on J_{HP} to 12 Hz, the number of experiments and the number of scans were 256. Correlation time (τ_c = 3.5 ns) was determined from H5-H6 NOESY crosspeaks for cytidines assuming isotropic motion.

The vicinal $^3J_{HP}$ have been obtained from DQF COSY spectra obtained with and without ^{31}P decoupling during aquisition time, and the projections in f2 dimension through cross peaks H3′-H4′ (down diagonal) have been taken. The sum of multiple splitting (Σ3′) in spectra obtained without ^{31}P decoupling is equal to $\Sigma(J_{3'4'} + J_{3'2''} + J_{3'2'} + J_{3'P})$ and with ^{31}P decoupling $\Sigma 3'(^{31}P)$ is equal to $\Sigma(J_{3'4'} + J_{3'2''} + J_{3'2'})$, $J_{3'P}$ has been determined as difference, $\Sigma 3' - \Sigma 3'(^{31}P)$ (see Figure 4, for example). In the second type of experiment, the ^{31}P-^1H correlation spectra have been obtained with double homonuclear decoupling on two frequencies: ν_1 for H2′ and H4′ (Note that the chemical shifts of H2′, and H4′are isochronous for T7, T8 residues, see Table I) and ν_2 for H2″. Taking the projection in f2 dimension through 3′P crosspeak the difference between positive and negative component of splitting represent the active coupling $J_{3'P}$ (see Figure 6A).

(iii) Duplex Structure Refinement

The starting coordinates of the duplexes were generated using the AMBER (v. 4.1) program (34, 45) from Arnott A- and B-DNA coordinates as well as from two X-ray structures with codes BDL001 (21) and BDLS79 (2) from the crystallographic Nucleic Acids Database (NDB, State University of New Jersey). Since the AMBER force field does not contain charges for the carbocyclic residue it was necessary to calculate them. To an X-ray structure (46) of carba-thymidine, a methyl group was added, which was used as the starting geometry for our *ab initio* geometry optimization. The Gaussian 94 program (47) was used for a geometry optimization (HF/6-31G* level), and for a calculation of electrostatic potential at points in space surrounding the molecule (using Merz-Kollman option and the 6-31G* basis set). The atom centered partial charges were calculated by the RESP program (48) and were averaged for few different sugar ring conformations (Figure 1B). The charges on 3′- and 5′-hydroxyl groups were set to be the same as in the common nucleotide residues (48) for consistency between the carbocyclic residues and the standard nucleotides.

The structure refinement was done using an iterative scheme similar to the scheme employed by Gorenstein *et al.* (49, 50). Each cycle of structure refinement involved an energy minimization and MD simulation of 14 ps (6 ps at 800 K, cooling to 300 K over a 4 ps period and then 4 ps at 300 K) using the SANDER module of the AMBER package. During the last 2 ps the atomic coordinates were saved at 250 fs intervals, the eight collected conformers were averaged, and then energy minimized. Distance constraints for AMBER were derived at each cycle from the experimental NOESY volumes using the iterative hybrid matrix procedure MARDI-

GRAS / RANDMARDI (v. 5.1)(32, 51). The results were combined and averaged for all interproton distances using the NOESY spectra in D_2O at different mixing times. Five cycles of MD/RANDMARDI refinement were used for each duplex starting structure. The constraints were weak (low force constants and wide flat bottoms of the potential wells) during the initial cycles and stronger in the final cycles in order to more gently force the molecule into the correct conformation.

Acknowledgements

The authors thank the Swedish Technical Research Council (TFR) and the Swedish Natural Science Research Council (NFR) for generous financial support. We are grateful to Wallenbergsstiftelsen, Forskningsrådsnämnden (FRN), and Uppsala University for funds for the purchase of a 500 and 600 MHz NMR spectrometers.

References and Foonotes

1. K.-H. Altmann, R. Kesselring and U. Pieles, *Tetrahedron*, 52, 12699-12722 (1996)
2. S. Portmann, K.-H. Altmann, N. Reynes and M. Egli, *J. Am. Chem. Soc.*, *119*, 2396-2403 (1997)
3. D. G. Knorre, V. V. Vlassov, V. F. Zarytova, A. V. Lebedev and O. S. Fedorova, *Design and Targeted Reactions of Oligonucleotide Derivatives.*, CRC Press, Boca Raton, FL., 1994
4. B. I. Schweitzer, T. Mikita, G. W. Kellogg, K. H. Gardner and G. P. Beardsley, *Biochemistry*, *33*, 11460-11475 (1994)
5. C. González, W. Stec, M. A. Reynolds and T. L. James, *Biochemistry*, *34*, 4969-4982 (1995)
6. Y. Cho, F. C. Zhu, L. B.A. and D. G. Gorenstein, *J. Biomol. Struct. Dynamics*, *11*, 685-702 (1993)
7. M. Egli, *Angew. Chem. Internat. Edit.*, *35*, 1894-1909 (1996)
8. (a) J. Chattopadhyaya, *Nucl. Acids Res. Symposium Ser.*, *35*, 111-112 (1996), (b) L. H. Koole, H. M. Buck, A. Nyilas and J. Chattopadhyaya, *Can. J. Chem.*, *65*, 2089-2094 (1987), (c) L. H. Koole, H. M.Buck, H. Bazin and J. Chattopadhyaya, *Tetrahedron*, *43*, 2989-2997 (1987), (d) L. H. Koole, J. Plavec, H. Liu, B. R. Vincent, M. R. Dyson, P. L. Coe, R. W. Walker, G. W. Hardy, S. G. Rahim and J. Chattopadhyaya, *J. Am. Chem. Soc.*, *114*, 9936-9943 (1992), (e) J. Plavec, L. H. Koole and J. Chattopadhyaya, *J. Biochem. Biophys. Meth.*, *25*, 253-272 (1992), (f) J. Plavec, W. Tong and J. Chattopadhyaya, *J. Am. Chem. Soc.*, *115*, 9734-9746 (1993), (g) J. Plavec, N. Garg and J. Chattopadhyaya, *J. Chem. Soc. Chem. Comm.*, 1011-1014 (1993), (h) J. Plavec, C. Thibaudeau, G. Viswanadham, C. Sund and J. Chattopadhyaya, *J. Chem. Soc. Chem. Comm.*, 781-783 (1994), (i) J. Plavec, C. Thibaudeau and J. Chattopadhyaya, *J. Am. Chem. Soc.*, *116*, 6558-6560 (1994), (j) J. Plavec, C. Thibaudeau, G. Viswanadham, C. Sund, A. Sandström and J. Chattopadhyaya, *Tetrahedron*, *51*, 11775-11792 (1995), (k) J. Plavec, C. Thibaudeau and J. Chattopadhyaya, *Pure Appl. Chem.*, *68*, 2137-2144 (1996), (l) C. Thibaudeau, J. Plavec, N. Garg, A. Papchikhin and J. Chattopadhyaya, *J. Am. Chem. Soc.*, *116*, 4038-4043 (1994), (m) C. Thibaudeau, J. Plavec and J. Chattopadhyaya, *J. Am. Chem. Soc.*, *116*, 8033-8037 (1994), (n) C. Thibaudeau, J. Plavec, K. A. Watanabe and J. Chattopadhyaya , *J. Chem. Soc. Chem. Comm.*, 537-540 (1994), (o) C. Thibaudeau, J. Plavec and J. Chattopadhyaya, *J. Org. Chem.*, *61*, 266-286 (1996), (p) I. Luyten, C. Thibaudeau, A. Sandström and J. Chattopadhyaya, *Tetrahedron*, *53*, 6433-6464 (1997)
9. W. Nerdal, D. R. Hare and B. R. Reid, *Biochemistry*, 28, 10008-10021 (1989)
10. K. Kaluarachchi, R. P. Meadows and D. G. Gorenstein, *Biochemistry*, *30*, 8785-8797 (1991)
11. F. J. M. van de Ven and C. W. Hilbers, *Eur. J. Biochem.*, *178*, 1-38 (1988)
12. A. M. Gronenborn and G. M. Clore, *Prog. Nucl. Magn. Reson. Spectrosc.*, *17*, 1-31 (1985)
13. S.-I. Yamakage, T. V. Maltseva, F. P. Nilsson, A. Földesi and J. Chattopadhyaya, *Nucl. Acids Res.*, *21*, 5005-5011 (1993)
14. A. Földesi, S.-I. Yamakage, T. V. Maltseva, F. P. R. Nilson, P. Agback and J. Chattopadhyaya, *Tetrahedron*, *51*, 10065-10092 (1995)
15. R. V. Hosur, G. Govil and H. T. Miles, *Magn. Reson. Chem.*, *26*, 927-944 (1988)
16. L. J. Rinkel and C. Altona, *J. Biomol. Struct. Dynamics*, *4*, 621-649 (1987)
17. E. Diez, J. S. Fabian, J. Guilleme, C. Altona and L. A. Donders, *Molec. Phys.*, *68*, 49 (1989)
18. L. A. Donders, F. A. A. M. de Leeuw and C. Altona, *Magn. Reson. Chem.*, *27*, 556 (1989)
19. C. Altona, J. H. Ippel, A. J. A. W. Hoekzema, C. Erkelens, G. Groesbeek and L. A. Donders, *Magn. Reson. Chem.*, *27*, 564 (1989)
20. L. H. Koole, J. Plavec, H. Liu, B. R. Vincent, M. R. Dyson, P. L. Coe, R. W. Walker, G. W. Hardy, S. G. Rahim and J. Chattopadhyaya, *J. Am. Chem. Soc.*, *114*, 9936-9943 (1992)
21. R. E. Dickerson and H. R. Drew, *J. Mol. Biol.*, *149*, 761 (1981)
22. S.-G. Kim, L.-J. Lin and B. R. Reid, *Biochemistry*, *31*, 3564-3574 (1992)
23. P. Schmieder, J. H. Ippel, H. van den Elst, G. A. van der Marel, J. H. van Boom, C. Altona and H. Kessler, *Nucl. Acids Res.*, *20*, 4747-4751 (1992)
24. J. Plavec and J. Chattopadhyaya, *Tetrahedron Lett.*, *36*, 1949-1952 (1995)
25. P. P. Lankhorst, C. A. G. Haasnoot, C. Erkelens and C. Altona, *J. Biomol. Struct. Dynamics*, *1*, 1387-1405 (1984)

26. V. K. Roongta, C. R. Jones and D. G. Gorenstein, *Biochemistry*, *29*, 5245-5258 (1990)
27. K. V. R. Chary, V. K. Rastogi and G. Govil, *J. Magn. Reson.*, *102 B*, 81-83 (1993)
28. M. Barfield, A. M. Dean, C. J. Fallick, R. J. Spear, S. Sternhell and P. W. Westerman, *J. Am. Chem. Soc.*, *97*, 1482-1492 (1975)
29. V. Sklenar and A. Bax, *J. Am. Chem. Soc.*, *109*, 7525-7526 (1987)
30. P. P. Lankhorst, C. A. G. Haasnoot, C. Erkelens, H. P. Westerink, G. A. van der Marel, J. H. van Boom and C. Altona, *Nucl. Acids Res.*, *13*, 927-942 (1985)
31. H. Liu, H. P. Spielmann, N. B. Ulyanov, D. E. Wemmer and T. L. James, *J. Biomol. NMR*, *6*, 390-402 (1995)
32. B. A. Borgias, P. D. Thomas, H. Liu, A. Kumar, M. Tonelli and T. L. James, MARDIGRAS 5.1 University of California, San Fransisco, CA, 1995
33. W. Saenger, *Principles of Nucleic Acids Structure.*; Springer-Verlag, New York, 1984
34. D. A. Pearlman, D. A. Case, J. C. Caldwell, W. S. Ross, T. E. Cheatham III, D. M. Ferguson, G. L. Seibel, U. C. Singh, P. K. Weiner and P. A. Kollman, AMBER 4.1, University of California, San Fransisco, CA, 1995
35. P. D. Thomas, V. J. Basus and T. L. James, *Proc. Natl. Acad. Sci. USA*, *88*, 1237-1241 (1991)
36. C. R. Calladine, *J. Mol. Biol.*, *161*, 343-352 (1982)
37. A. V. Fratini, M. L. Kopka, H. R. Drew and R. E. Dickerson, *J. Biol. Chem.*, *257*, 14686-14707 (1982)
38. O. Kennard and W. N. Hunter, *Angew. Chem. Internat. Edit.*, *30*, 1254-1277 (1991)
39. M. S. Babcock, E. P. D. Pednault and W. K. Olson, *J. Mol. Biol.*, *237*, 125-156 (1994)
40. Y. Duan, P. Wilkosz, M. Crowley and J. M. Rosenberg, *J. Mol. Biol.*, *272*, 553-572 (1997)
41. T. V. Maltseva, K.-H. Altman, M. Egli and J. Chattopadhyaya, *J. Mol. Biol.*, (1998)
42. B. A. Luxon and D. G. Gorenstein, in *Methods in Enzymology*, *261*, T. L. James (Ed.), Academic Press, San Diego, CA., 1995, pp. 45-73
43. N. B. Ulyanov and T. L. James, in *Methods in Enzymology*, *261*, T. L. James (Ed.), Academic Press, San Diego, CA., 1995, pp. 90-120
44. H. R. Drew, R. M. Wing, T. Takano, C. Broka, S. Tanaka, K. Itakura and R. E. Dickerson, *Proc. Natl. Acad. Sci. USA*, *78*, 2179-2183 (1981)
45. W. D. Cornell, P. Cieplak, C. I. Bayly, I. R. Gould, K. M. Merz Jr., D. M. Ferguson, D. C. Spellmeyer, T. Fox, J. W. Caldwell and P. A. Kollman, *J. Am. Chem. Soc.*, *117*, 5179-5197 (1995)
46. A. Kalman, T. Koritsanszky, J. Beres and G. Sagi, *Nucleosides & Nucleotides*, *9*, 235-243 (1990)
47. M. J. Frisch, G. W. Trucks, H. B. Schlegel, P. M. W. Gill, B. G. Johnson, M. A. Robb, J. R. Cheeseman, T. A. Keith, G. A. Petersson, J. A. Montgomery, K. Raghavachari, M. A. Al-Laham, V. G. Zakrzewski, J. V. Ortiz, J. B. Foresman, J. Cioslowski, B. B. Stefanov, A. Nanayakkara, M. Challacombe, C. Y. Peng, P. Y. Ayala, W. Chen, M. W. Wong, J. L. Andres, E. S. Replogle, R. Gomperts, R. L. Martin, D. J. Fox, J. S. Binkley, D. J. Defrees, J. Baker, J. P. Stewart, M. Head-Gordon, C. Gonzalez and J. A. Pople, Gaussian 94 Rev. C.3, Gaussian Inc., Pittsburgh, PA, 1995
48. P. Cieplak, W. D. Cornell, C. Bayly and P. A. Kollman, *J. Comp. Chem.*, *16*, 1357-1377 (1995)
49. K. Kaluarachchi, R. P. Meadows and D. G. Gorenstein, *Biochemistry*, *30*, 8785-8797 (1991)
50. E. P. Nikonowicz, R. P. Meadows, P. Fagan and D. G. Gorenstein, *Biochemistry*, *30*, 1323-1334 (1991)
51. B. A. Borgias and T. L. James, *J. Magn. Reson.*, *87*, 475-487 (1990)

Date Received: June 16, 1998

Communicated by the Editor Ramaswamy H. Sarma